

# SANDIA REPORT

SAND86-2164 • UC-60

Unlimited Release

Printed October 1987

98-8232-2166389

*Cy 1*



8232-2/066389



00000001 -

## Measurements and Calculations of Aerodynamic Torques for a Vertical-Axis Wind Turbine

Robert E. Akins, Dale E. Berg, W. Tait Cyrus

Prepared by  
Sandia National Laboratories  
Albuquerque, New Mexico 87185 and Livermore, California 94550  
for the United States Department of Energy  
under Contract DE-AC04-76DP00789

|

Issued by Sandia National Laboratories, operated for the United States Department of Energy by Sandia Corporation.

**NOTICE:** This report was prepared as an account of work sponsored by an agency of the United States Government. Neither the United States Government nor any agency thereof, nor any of their employees, nor any of their contractors, subcontractors, or their employees, makes any warranty, express or implied, or assumes any legal liability or responsibility for the accuracy, completeness, or usefulness of any information, apparatus, product, or process disclosed, or represents that its use would not infringe privately owned rights. Reference herein to any specific commercial product, process, or service by trade name, trademark, manufacturer, or otherwise, does not necessarily constitute or imply its endorsement, recommendation, or favoring by the United States Government, any agency thereof or any of their contractors or subcontractors. The views and opinions expressed herein do not necessarily state or reflect those of the United States Government, any agency thereof or any of their contractors or subcontractors.

Printed in the United States of America  
Available from  
National Technical Information Service  
U.S. Department of Commerce  
5285 Port Royal Road  
Springfield, VA 22161

NTIS price codes  
Printed copy: A03  
Microfiche copy: A01

# Measurements and Calculations of Aerodynamic Torques for a Vertical-Axis Wind Turbine

Robert E. Akins  
Washington and Lee University  
Lexington, VA 24450

Dale E. Berg  
Wind Energy Research Division  
Sandia National Laboratories  
Albuquerque, NM 87185

W. Tait Cyrus  
Bureau of Engineering Research  
University of New Mexico  
Albuquerque, NM 87131

## Abstract

This report describes measurements of aerodynamic torque on a vertical-axis wind turbine. Accelerometers mounted at the equator of the rotor and a torque meter mounted at the base of the rotor were used to compute the net aerodynamic torque acting on the rotor. Assumptions concerning blade-response symmetry were required to achieve blade torque as a function of rotor position on each half of a revolution for a two-bladed rotor. Results are presented for tip-speed ratios from 2.5 to 8.0 for two turbine rotational speeds. Evidence of dynamic stall is observed at low tip-speed ratios.



# Contents

1. Introduction .....	7
2. Background .....	8
3. Measurements and Data Reduction .....	10
3.1 Instrumentation .....	10
3.2 Data Collection .....	11
3.3 Corrections and Adjustments to Data .....	11
3.4 Data Reduction .....	12
4. Calculation of Aerodynamic Torque .....	17
4.1 SIDIF Model .....	17
4.2 Dynamic Stall Model .....	17
5. Results .....	18
5.1 Results for 38.7 rpm .....	18
5.2 Results for 50.6 rpm .....	27
5.3 Fourier Coefficients .....	33
6. Conclusions .....	36
References .....	37

## Figures

1 Free-body diagram of rotor used in rigid-body approximation .....	8
2 SANDIA/DOE 17-m research turbine, Albuquerque, New Mexico .....	9
3 Nomenclature used in defining relative rotor position .....	12
4 Comparison between relative rotor positions 0° to 180° and 180° to 360°, 50.6 rpm, TSR 2.87 .....	14
5 Comparison between relative rotor positions 0° to 180° and 180° to 360°, 50.6 rpm, TSR 5.08 .....	15
6 Standard deviations of aerodynamic torques in a bin, 50.6 rpm, TSR 2.87 .....	15
7 Standard deviations of aerodynamic torques in a bin, 50.6 rpm, TSR 5.08 .....	16
8 Aerodynamic torque as a function of tip-speed ratio, 38.7 rpm, TSR 2.20 to 3.89 .....	19
9 Aerodynamic torque as a function of tip-speed ratio, 38.7 rpm, TSR 3.89 to 7.98 .....	19
10 Aerodynamic torque as a function of tip-speed ratio, 38.7 rpm, TSR 2.02 and 2.08 .....	21
11 Aerodynamic torque as a function of tip-speed ratio, 38.7 rpm, TSR 2.14 and 2.20 .....	21
12 Aerodynamic torque as a function of tip-speed ratio, 38.7 rpm, TSR 2.26 and 2.33 .....	22
13 Aerodynamic torque as a function of tip-speed ratio, 38.7 rpm, TSR 2.41 and 2.49 .....	22
14 Comparison between measured and predicted aerodynamic torque, 38.7 rpm, TSR 2.5 .....	24
15 Comparison between measured and predicted aerodynamic torque, 38.7 rpm, TSR 3.0 .....	24
16 Comparison between measured and predicted aerodynamic torque, 38.7 rpm, TSR 3.5 .....	25
17 Comparison between measured and predicted aerodynamic torque, 38.7 rpm, TSR 4.0 .....	25
18 Comparison between measured and predicted aerodynamic torque, 38.7 rpm, TSR 4.5 .....	26
19 Comparison between measured and predicted aerodynamic torque, 38.7 rpm, TSR 5.5 .....	26
20 Comparison between measured and predicted aerodynamic torque, 38.7 rpm, TSR 6.5 .....	27
21 Aerodynamic torque as a function of tip-speed ratio, 50.6 rpm, TSR 2.87 to 4.61 .....	28
22 Aerodynamic torque as a function of tip-speed ratio, 50.6 rpm, TSR 4.61 to 7.93 .....	28
23 Comparison between measured and predicted aerodynamic torque, 50.6 rpm, TSR 2.5 .....	30
24 Comparison between measured and predicted aerodynamic torque, 50.6 rpm, TSR 3.0 .....	30
25 Comparison between measured and predicted aerodynamic torque, 50.6 rpm, TSR 3.5 .....	31

## Figures (continued)

26	Comparison between measured and predicted aerodynamic torque, 50.6 rpm, TSR 4.0 .....	31
27	Comparison between measured and predicted aerodynamic torque, 50.6 rpm, TSR 4.5 .....	32
28	Comparison between measured and predicted aerodynamic torque, 50.6 rpm, TSR 5.5 .....	32
29	Comparison between measured and predicted aerodynamic torque, 50.6 rpm, TSR 6.5 .....	33
30	Fourier coefficients of torque, 38.7 rpm .....	34
31	Fourier coefficients of torque, 50.6 rpm .....	35

## Tables

1	Aerodynamic torques in N-M, 38.7 rpm .....	20
2	Aerodynamic torques in N-M, 38.7 rpm .....	23
3	Aerodynamic torques in N-M, 50.6 rpm .....	29
4	Fourier coefficients of torque, 38.7 rpm .....	33
5	Fourier coefficients of torque, 50.6 rpm .....	34

# Measurements and Calculations of Aerodynamic Torques for a Vertical-Axis Wind Turbine

## 1. Introduction

The ability to understand and accurately predict the aerodynamic forces acting on a wind turbine is an essential step in the design process. In the past ten years, substantial progress has been made in gaining a better understanding of the aerodynamics of vertical-axis wind turbines (VAWTs). In the past, the prime quantity against which the analytical models were verified and validated was the output power or torque averaged over an entire revolution of the rotor. This measure was initially a logical method of checking the accuracy of the model and its assumptions, but many of the advanced aspects of design require more information. Of particular importance are the variations of the torque or power during the rotor rotation.

Considerable effort has been devoted to the development of enhanced capabilities to predict the effects of dynamic stall on VAWTs, but most data available to guide these efforts are based on an entire rotation. A torque or power that has been integrated over an entire rotation does not show the effects of a phenomenon that occurs only for a small portion of the rotation. The effects of dynamic stall on the torque produced by the rotor are a function of rotor position, and these effects will be evident only for a portion of the rotation. In addition, the frequency content of the torque is a key element in the analysis of the structural dynamics of the rotor. Any variation in the aerodynamic torque during a rotation contributes to the frequencies affecting the response of the rotor.

To measure the aerodynamic torque applied to a rotor, an experimental program was developed. The DOE/Sandia 17-m research VAWT located in Albuquerque, New Mexico, was instrumented with triaxial accelerometers at the equator of each blade. In addition to these transducers, the net torque on the rotor, wind speed, wind direction, rotor position, and additional relevant parameters were measured. The instrumentation used did not allow the determination of the local force acting on a blade element. To calculate the applied aerodynamic torque, certain simplifying assumptions were required to account for the motion of the drivetrain and to isolate the rotor from the remainder of the wind turbine. The rotor is assumed to act as a rigid body and, therefore, to have the same acceleration over the entire rotor. Aerodynamic effects are integrated over the length of the blade and summed up for all the blades (in this instance, two). With these assumptions, the accelerometer measurements were used to calculate the net aerodynamic torque applied to the VAWT as a function of rotor position. This approach will provide only the aerodynamic torque averaged over the entire rotor.

Our major goal was to obtain a measurement of the applied aerodynamic torque for various operating conditions of the wind turbine.

## 2. Background

A VAWT has a soft drive train, that is, the rotor is much stiffer in torsion than the low-speed shaft (the shaft that connects the rotor to the transmission or speed increaser). A soft system damps out torque variations at high frequencies. This feature results in a more uniform power output than that produced by a stiffer system, and also causes differences between the output power and the applied aerodynamic torques. Because the torsional stiffness of the rotor is much greater than that of the low-speed shaft, the rotor's torsional response may be assumed to be simple rigid-body motion. A free-body diagram of the rotor is shown in Figure 1. Using this diagram and summing moments about the vertical axis, the following equation is obtained:

$$T_a(t) - T_l(t) = J_r \ddot{\theta}(t) \quad , \quad (1)$$

where

$J_r$  = the mass moment of inertia of the rotor (kg-m<sup>2</sup>)

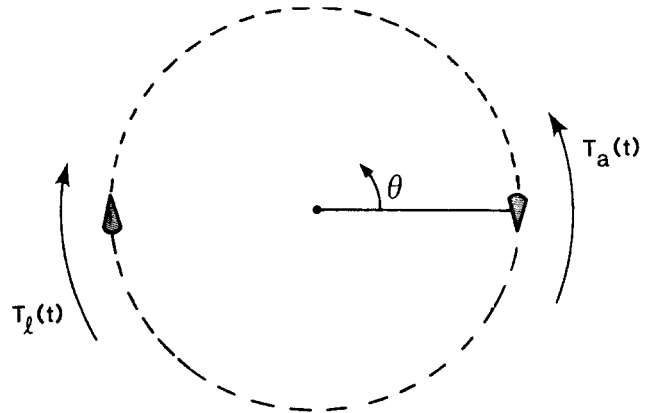
$T_a(t)$  = the aerodynamic forcing function (n-m)

$T_l(t)$  = the measured torque on the low-speed shaft at the base of the rotor (n-m)

$\ddot{\theta}(t)$  = the rigid-body angular acceleration of the rotor (rad/sec<sup>2</sup>).

For the configuration used in this study,  $\ddot{\theta}(t)$  was measured with the accelerometers,  $T_l(t)$  was measured with a torque sensor mounted on the low-speed shaft, and  $J_r$  was calculated for the 17-m rotor to be 40 620 kg-m<sup>2</sup>. To obtain the angular acceleration with accelerometers that measure a linear acceleration, it was necessary to divide the linear tangential acceleration by the radius of the turbine. This assumption was crucial to the data reduction used in the study. The rotor does deform somewhat during operation and is not a true rigid body. However, the magnitudes of the accelerations due to the deformation are substantially less than the accelerations due to the rigid-body motion, and are therefore ignored in the data reduction. This assumption is a limitation in the quality and accuracy of the results. In addition, if Eq (1) is solved for  $T_a(t)$ , the resulting expression is the difference between two large numbers. Errors in the measurement of either  $T_l$  or  $\ddot{\theta}$  will therefore have a large effect

on the calculated value of  $T_a$ . This approach was first used by McNerney<sup>1</sup> in a similar but less detailed study.



ROTOR VIEWED FROM TOP

$$T_a(t) - T_l(t) = J_r \ddot{\theta}(t)$$

Figure 1. Free-body diagram of rotor used in rigid-body approximation

With these assumptions,  $T_a$ , the aerodynamic torque, was determined as a function of rotor position for any given wind speed or corresponding tip-speed ratio TSR (TSR = blade rotational velocity at equator/undisturbed wind speed). The aerodynamic models predict this torque locally and then integrate over the blade to obtain the total torque acting on the blade. The torque contributions from each blade are then added to get the total torque produced by the rotor. For the two-bladed VAWT configuration used in this study, the values obtained for  $T_a$  repeat every 180° of turbine rotation. Because of the rigid-body assumption, it is impossible to separate the upwind/downwind differences in  $T_a$ . This aspect of the measurements makes it difficult to interpret the results, particularly with respect to phenomena such as dynamic stall that occur only for a small portion of the rotation. Nevertheless, the results provide an improved method of interpreting the tangential forces induced by the aerodynamic loads.

To compare the measurements with at least one version of the current aerodynamic models, the double-multiple stream-tube (DMS) model<sup>2</sup> currently

in use at Sandia National Laboratories was used to predict the total torque for the entire rotor. This model is based on the concept originally developed by Paraschivoiu.<sup>3</sup> The model and the parameters used in the calculations are discussed in greater detail in Section 4.

All measurements were obtained using the DOE/Sandia 17-m research VAWT. This turbine is shown in Figure 2 and is discussed in detail in Johnston.<sup>4</sup> The

configuration used during these tests consisted of two blades with a height-to-diameter ratio of 1.0. The blades were NACA 0015 with a chord of 0.612 m (2.0 ft) and were attached to the tower at the roots only; no struts were used in this particular design. The blades were bent from a single extrusion; there were no blade-to-blade joints. Ground clearance of the rotor was 4.88 m (16.0 ft); maximum rotor radius was 8.36 m (27.3 ft) with a swept area of 187.1 m<sup>2</sup> (2000 ft<sup>2</sup>).

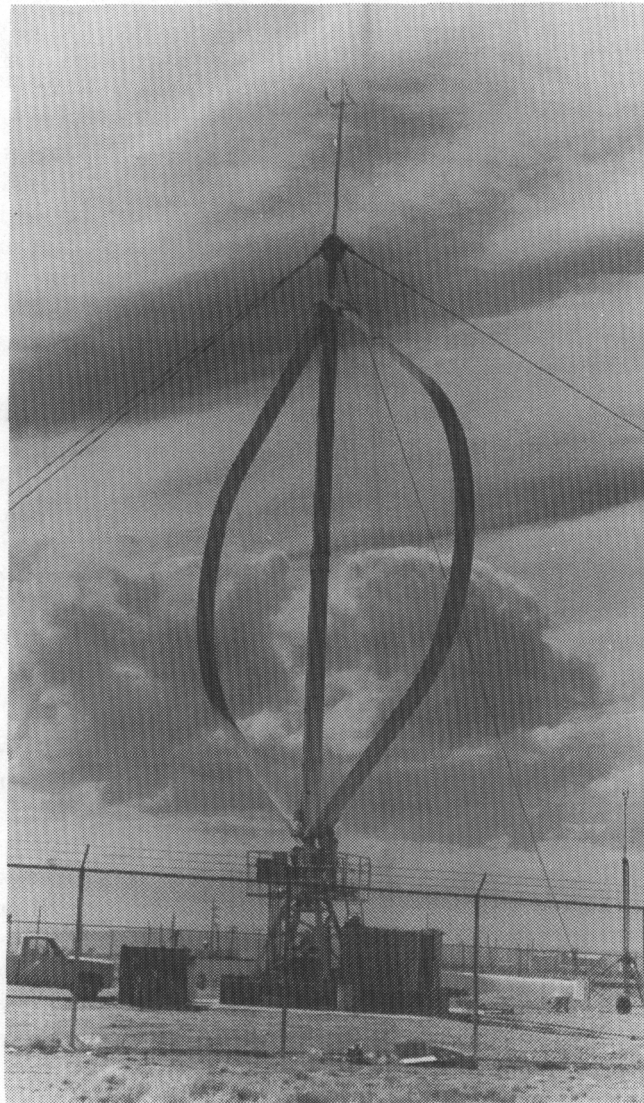


**Figure 2.** SANDIA/DOE 17-m research turbine, Albuquerque, New Mexico

## 3. Measurements and Data Reduction

Any measurement on an operating wind turbine represents a difficult task, mainly because of the random nature of the wind and the general unsteady nature of the entire process. This program was no exception. Many difficulties were encountered in setting up the experiment, and more problems surfaced in the data reduction. Many of these difficulties are outlined in the following sections, but it is important to understand these problems in considering the data presented in Section 5. Values of aerodynamic torque or rotor position relative to the incident wind are subject to substantial uncertainty, but general trends that may be considered definitive are evident. The most important approximation is the measurement of wind speed and direction above the turbine, as these values are considered representative of the incident wind experienced by the entire rotor. The wind speed is corrected to a value at the center of the rotor using the average wind shear at the site.

### 3.1 Instrumentation

A brief description of all key components of the instrumentation is important in understanding and interpreting the results. Key instruments are summarized below, and important features are emphasized.

#### 3.1.1 Accelerometers

Three accelerometers were mounted at the equator or midheight point of each blade. A mounting bracket allowed all three to be mounted close to a common point. For one blade, the accelerometers were mounted inside the blade using access provided for another concurrent experiment. The accelerometers were mounted on the outside of the second blade, and were enclosed in a faired container to reduce the additional drag on the fixture. The accelerometers used were the Schaevitz SM series with tangential and vertical-component full-scale ranges of 2 g's and radial-component full-scale values of 25 g's (due to the centrifugal accelerations while the turbine is in operation). The accelerometers were calibrated before installation on the turbine.

#### 3.1.2 Wind Speed and Direction

A cup-vane anemometer system was mounted on a tower extending from the top of the turbine. This system has been used in all past performance measurements on this wind turbine and has been extremely useful. The transducers are not significantly influenced by the operation of the wind turbine.<sup>5</sup> The anemometer used was a Teledyne Geotech Model 1564B, with a distance constant of 1.5 m (5 ft) of air. The corresponding vane, Model 1565B, had a distance constant of 0.5 m (1.6 ft) of air and a damping ratio of 0.2 at a 10° initial angle of attack. The signal conditioning associated with the cup-vane systems was calibrated weekly during the test period. The total system was not calibrated in a wind tunnel but was replaced with new instrumentation when any problems with bearings, cups, or vanes were noted.

#### 3.1.3 Rotor Position

The rotor position was monitored with an AST/SERVO Systems synchro system attached to the base of the rotor with a chain drive. The electrical signal was fed into the instrumentation system along with other signals. A synchro-to-dc converter was used to transform the information from a three-wire synchro source to a dc analog voltage proportional to the synchro shaft angle.

#### 3.1.4 Torque Transducer

A Lebow torque transducer, consisting of a strain-gage bridge, a tachometer, and associated slip rings, was mounted in the low-speed shaft at the base of the rotor. The unit operates on an ac carrier and uses external signal conditioning to convert the signals into dc analog voltages. This unit was calibrated annually by removing it from the turbine and applying dead loads in a calibration fixture. The signal conditioning equipment was adjusted weekly, using calibration resistors.

### 3.1.5 Pulse Code Modulator System

A 64-channel pulse code modulator (PCM) system is part of the standard instrumentation at the VAWT test facility. The PCM system takes multiple analog data channels (i.e., accelerometers) and converts them into a single, high-level, serial data stream. This high-level data stream passes through slip rings at the base of the wind turbine and into the data acquisition system. The system results in a lower noise-to-signal ratio than would be the case were the low-level signals to pass through the slip rings. Important ground-based signals such as the rotor position, wind speed, and direction and torque at the low-speed shaft were fed through slip rings into the PCM so that all important signals could be digitized simultaneously.

## 3.2 Data Collection

The turbine uses the frequency of the utility grid to operate the generator at a constant speed. The configuration of the system with a belt and pulley on the turbine high-speed shaft allows the rotor to operate at several discrete speeds. For this experiment, the rotor operated at 38.7 and 50.6 rpm. Data were collected on all channels at a rate of 50 samples per second, which corresponds to a minimum of 59 samples per revolution at the higher rotation rate. Data collection took place over a 9-month period. Conditions were selected to obtain records at wind speeds spanning the entire range of operation of the turbine. Data were collected in 12-minute records, limited by the capacity of the disk storage. A total of 22 records was collected at 38.7 rpm and 15 records at 50.6 rpm. These records were stored on hard disks and later analyzed on a Hewlett-Packard 1000 minicomputer. Data-reduction techniques are outlined in Section 3.4.

## 3.3 Corrections and Adjustments to Data

Because of the nature of the test and operational difficulties with several of the transducers, several key data channels had to be adjusted or corrected as a part of the data reduction. Some of these corrections have important implications in the interpretation of the data, and are summarized in the following sections.

### 3.3.1 Torque Measurements

The torque measurements on the low-speed shaft were adjusted in two ways. In the first correction, a tare torque was added to account for the friction in the system. This value was determined by spinning the rotor with no blades, and represented  $<5\%$  of the

peak torque, even at low wind speeds. The second correction was to adjust the zero-rpm reading for drift of the transducer. Before and after each data run, a short record of all transducers was taken with the turbine parked. This gave the current value of the "no load" reading of the torque transducer, which represented at most 5% of the peak torque reading. This value was used later in the data reduction to adjust the torque signal by a constant offset. The variation in the "no load" reading was due primarily to temperature variations at the test location.

### 3.3.2 Accelerometer Alignment

The accelerometers were mounted on an existing turbine in a field environment and exact alignment was not possible. Because the radial accelerations were much greater than the tangential accelerations, a small misalignment that would create only small relative errors in the radial measurement could introduce substantial errors in the tangential measurement by adding a radial component. Since the rotor operated in a constant-speed mode, the tangential acceleration averaged over several rotor revolutions should be zero. For each blade, an average value of the tangential acceleration was computed, based on several records at each operating rpm. These averages were constant for a given rpm and were independent of wind speed. Using the constant radial acceleration for each case, the average tangential acceleration was used to calculate a component due to the off-axis error in mounting the accelerometers. For the tangential accelerometers on the two blades, these errors were  $1.07^\circ$  and  $1.80^\circ$ . These mounting errors were independent of rpm and very repeatable. A constant correction (a function of rpm only) was applied to the tangential accelerometer reading to account for these errors.

### 3.3.3 Rotor Position Indicator

One of the key independent variables in this experiment was the rotor position relative to the incident wind. The synchro system provided a continuous analog indication of the absolute rotor position with a sawtooth signal that reset each revolution. Two major problems occurred that required corrections to the raw signal. The first problem was that the time interval for the synchro signal to reset was greater than the sample interval of  $1/50$  of a second. This caused several samples of rotor position to be in error for each rotation. The data reduction algorithm was modified to correct these errors and checked to ensure that the corrections did not alter the rotational period of the turbine. A more important problem was caused by slippage of the synchro relative to the rotor. Because

the data were analyzed extensively only after completion of the test, this difficulty was not apparent during data collection. To salvage as much data as possible, a correction was made based on the combination pitot-static/yaw probe located on the blade to measure the relative angle of attack. As the blade moved directly into the wind, the angle of attack changed sign. This change in sign and the instantaneous reading of wind direction from the top of the turbine were used to determine when the rotor position indicator should have reset for each rotation of the turbine, and a rotor offset error was calculated. This routine was checked on some of the earlier runs, when the transducer was operating properly, and found to be adequate. Using this technique, the zero reading or position-indicator offset was updated at each rotor revolution. The variation of this correction for each 12-minute data record was examined, and whenever anomalous behavior was noted the record was excluded from the composite data reduction.

Another check on the validity of these corrections was furnished by the periodicity of the data, i.e., the data repeating every  $180^\circ$  as the turbine rotated. As explained in Section 3.4, the data were sorted as a function of rotor position in  $6^\circ$  increments or bins. This wide band resulted in a large number of points in each bin and a good definition of the mean torque for each bin. The corrections were consistent and, at most, would cause an error of  $\pm 1$  rotor position increment ( $6^\circ$ ).

### 3.3.4 Wind Shear

The wind speed measured above the turbine was adjusted to an equivalent wind speed at the turbine centerline, using the average wind shear measured at the test facility.<sup>6</sup> A power-law exponent of 0.1 was used, reducing the measured wind speed by a factor of 0.91 to obtain the equatorial wind speed. This adjustment was applied before data reduction. Because the reference anemometer was located directly above the rotor, no corrections for lack of spatial correlation of wind speed were used.

### 3.3.5 Density Correction

To account for density changes, both the measured torque on the low-speed shaft and the torque derived from the accelerometer measurements were adjusted to a reference density of  $1.00 \text{ kg/m}^3$  ( $0.0625 \text{ lbm/ft}^3$ ) by multiplying the actual torque by the ratio of that reference density to the actual density at the time of measurement.

## 3.4 Data Reduction

Based on past experience with similar performance measurements, an approach based on the Method of Bins<sup>7-9</sup> was used to reduce the data.

### 3.4.1 Bins Approach

To determine the aerodynamic torque as a function of both mean wind speed and rotor position, a two-dimensional application of the Method of Bins was required. As in performance measurements, the measured torques were separated by instantaneous wind speed into bins  $0.447 \text{ m/s}$  ( $1.0 \text{ mph}$ ) wide. In reducing and reporting the data, these values were converted to a tip-speed ratio, a nondimensional parameter that is the ratio of the speed of the blade at the equator (tip) to the reference wind speed.

Based on the higher operating speed ( $50.6 \text{ rpm}$ ) of the rotor and the corresponding 59 samples per rotation, a  $6^\circ$  increment in rotor position was selected for sorting (or "binsing") with respect to rotor position. This increment is the smallest justified by the sample rate, and it is sufficiently small to resolve behavior as a function of rotor position. Relative rotor position is defined in Figure 3. A relative rotor position of  $0^\circ$  corresponds to the reference blade heading into the incident wind. The relative rotor position is a function of the absolute rotor position and the incident wind direction measured above the turbine, both of which are changing as a function of time.

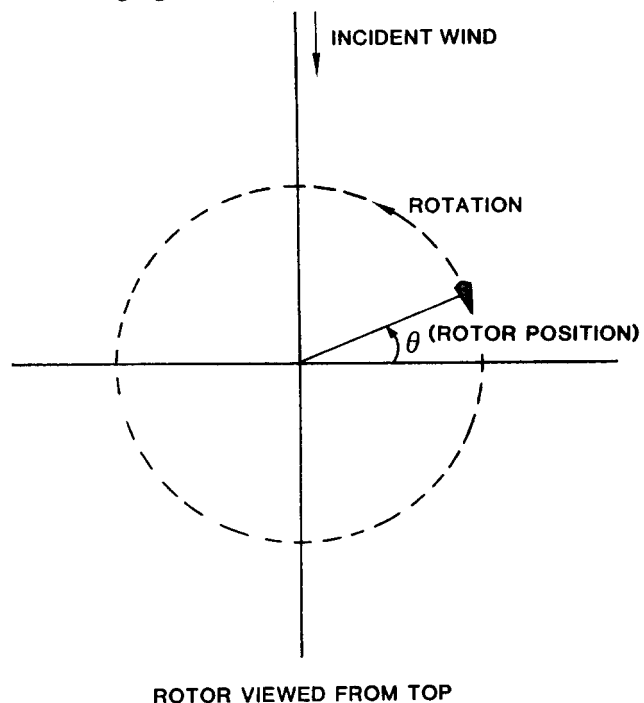


Figure 3. Nomenclature used in defining relative rotor position

The general pattern of data reduction was based on an array dimensioned  $3 \times 36 \times 50$ . The first dimension was used for each combination of reference wind speed and relative rotor position to store three quantities: (1) the number of readings for the combination, (2) the sum of the readings, and (3) the sum of the square of the readings. For each sample of data, the appropriate subscripts corresponding to the wind speed and relative rotor position were computed and these quantities updated to include the corresponding values for the sample. After a run, the sum of the readings for a given wind speed and rotor position was divided by the number of readings to obtain the average value. The sum of the squares was combined with the average value and the number of readings to obtain the standard deviation associated with the particular combination of wind speed and relative rotor position. This is the standard deviation of all instantaneous readings that fall into the corresponding range of wind speed and relative rotor position and is not indicative of the error of the measurements. The mean values computed using this technique repeat with variations less than the standard deviations of the readings in a particular bin.

Because the measurements were required as a function of rotor position, none of the advantages gained by averaging as a function of time (outlined in Akins<sup>8</sup>) were used. Consequently, considerable data from records with different mean wind speeds were collected and combined to obtain enough data for statistically valid results. This limitation also introduced some spreading of the data with respect to wind speed and rotor position.<sup>8</sup>

### 3.4.2 Individual Records

Initially, each data record was reduced separately. Both the measured torque on the low-speed shaft and the torque based on the tangential accelerometer readings were computed for each sample, and the aerodynamic torque was computed using Eq (1). Because the rotor was assumed to be rigid body, the accelerometer on either blade should have provided the same reading. This assumption was checked on several runs and was found to be valid. Instead of taking one or the other of the blades as the primary reading, the readings from both tangential accelerometers were averaged and this average used in the calculation of the aerodynamic torques. As indicated in Section 3.3.4, the reference wind speed was corrected for the mean shear prior to sorting the data as a function of wind speed and relative rotor position. The symmetry of the assumptions used in the data reduction will cause the results to repeat every  $180^\circ$ .

We expected the volume of data and the bins approach to be adequate to define the aerodynamic torque as a function of rotor position.

As stated in Section 3.3.5, both the low-speed torque and the torque calculated from the accelerometer readings were adjusted to a standard density before data reduction. Each record was reduced, and the summarized data stored on disk in a master file to be later retrieved and combined with other data.

### 3.4.3 Combined Records

After all data records at a particular rpm were reduced, a second program combined the results into a composite record. The techniques for this combination are outlined in Ref. 7. The data had already been corrected to a site-standard density, and no further corrections were made. Once this final compilation was obtained, data for the two operating rpms as a function of wind speed were available for analysis and comparison. Because of the wide range of wind speeds, none of the individual records was examined in detail. The number of data points in any particular bin for an individual record was not adequate to define the variation of torque with either rotor position or mean wind speed.

To relate these measurements to previous measurements, the torques for the combined results were averaged for an entire revolution and used to compute a turbine performance coefficient,  $C_p$ . This coefficient is defined as

$$C_p = \frac{(T\omega)}{(1/2\rho V^3A)} \quad (2)$$

where

$T$  = the average torque for a rotation

$\omega$  = the angular velocity of the rotor

$\rho$  = the density of air

$V$  = the incident wind speed

$A$  = the swept area of the rotor.

### 3.4.4 Typical Results and Repeatability of Data

Because sources of error are associated with the transducers, the corrections to the data, and the random nature of the process being studied, the reliability of the data is of concern. One empirical method of assessing the repeatability, if not the accuracy, of the data is to compare different measurements of the same quantities. This comparison does not allow the detection of any systematic errors in either measure-

ment or data reduction. It does, however, seem to be the best overall way to assess the accuracy of the results.

Because of the symmetry of the data, one comparison is to examine data for each half of a rotation. These results are shown in Figures 4 and 5 for two different tip-speed ratios at an operating speed of 50.6 rpm. Figure 4, for a tip-speed ratio of 2.87, corresponds to a high power output of the turbine. Data are shown for the first half of the rotation ( $0^\circ$  to  $180^\circ$ ) and compared with the second half of the rotation ( $180^\circ$  to  $360^\circ$ ). No substantial differences are evident in the two sets of data. The agreement in the range  $20^\circ$  to  $60^\circ$  ( $200^\circ$  to  $240^\circ$ ), where there is a relatively steep slope in the curve, is a good indication that any corrections to the relative rotor position were consistent. If an incorrect offset were introduced, it would have been most evident in this portion of the curve. A second comparison of data at a higher tip-speed ratio and much lower power production is shown in Figure 5. Again, no substantial differences are evident in the two sets of data.

Another measure of the spread of data obtained using the Method of Bins is the standard deviation of the values in a particular bin. This bin standard deviation is usually much larger than the difference between two measurements such as was shown in

Figures 4 and 5. The bin standard deviation is not an error band that might be measured in a deterministic measurement. The variability in the values in a bin is due to a combination of measurement errors and the random nature of the process being observed. One interpretation of the bin standard deviation is that it indicates a 66.7% probability that any instantaneous observation of a variable (for example, the torque) will fall within this value of the mean. Figure 6 shows the mean values (+'s) and one standard deviation greater than and less than the mean values (solid lines). These data are for a tip-speed ratio of 2.87 at an operating rpm of 50.6. The data shown in Figure 4 on a similar scale have significantly less variation than that indicated by the bin standard deviation. A similar set of data for a tip-speed ratio of 5.08 and an operating rpm of 50.6 is shown in Figure 7. The mean values are substantially less than those in Figure 6, yet the bin standard deviations are comparable.

Although it is not possible to make a definitive statement about the accuracy of the data, these two representations certainly provide an estimate of the repeatability, which is the best measure of the quality of the data. Based on these values, an estimate of accuracy of 10% of the reading or 5% of peak torque seems appropriate.

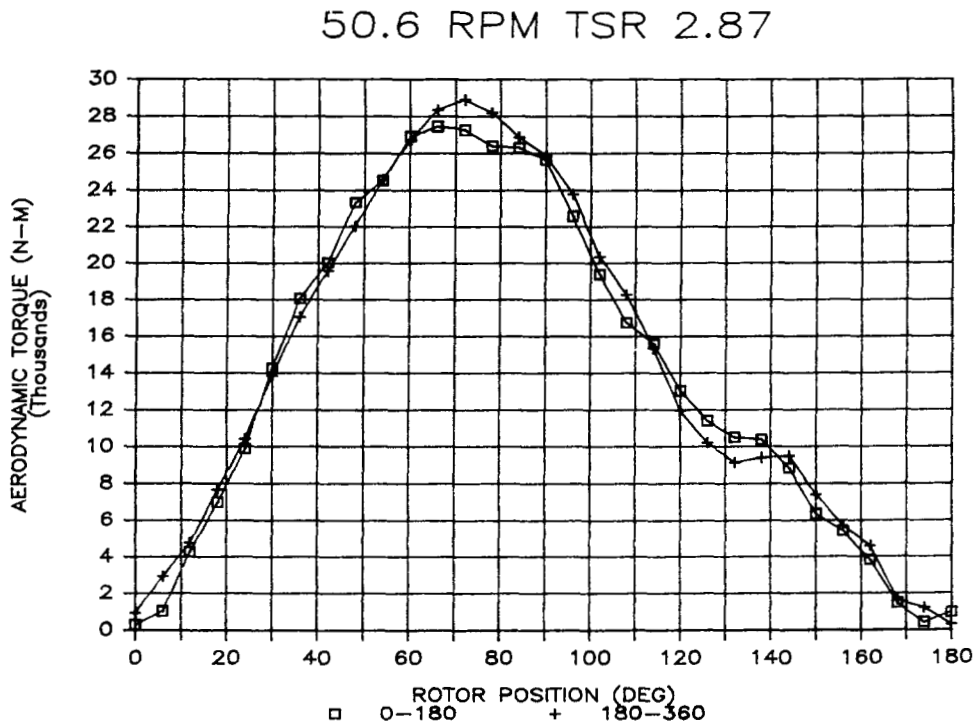


Figure 4. Comparison between relative rotor positions  $0^\circ$  to  $180^\circ$  and  $180^\circ$  to  $360^\circ$ , 50.6 rpm, TSR 2.87

50.6 RPM TSR 5.08

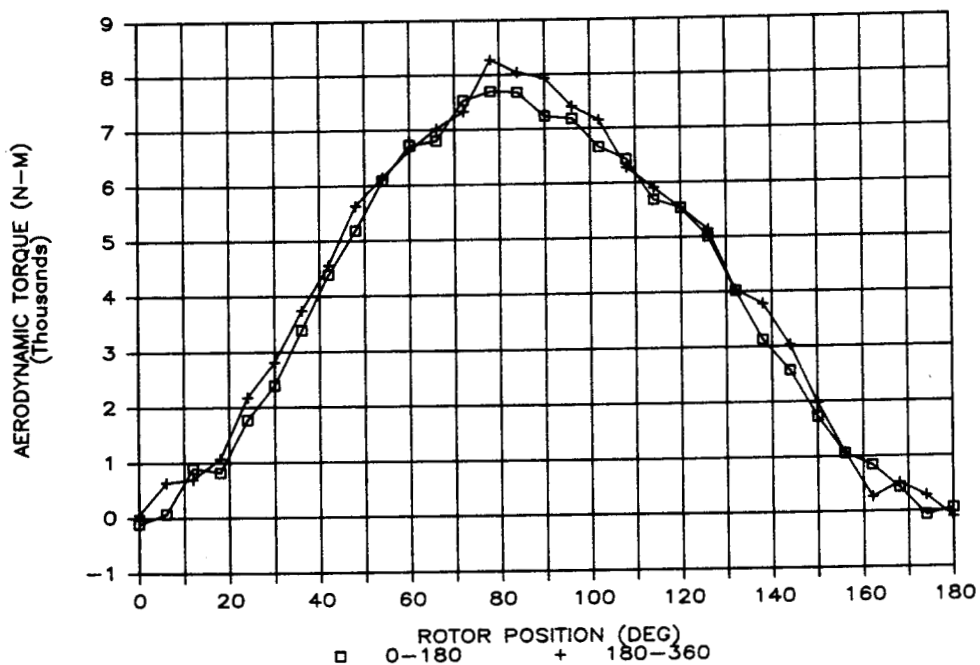


Figure 5. Comparison between relative rotor positions 0° to 180° and 180° to 360°, 50.6 rpm, TSR 5.08

50.6 RPM TSR 2.87

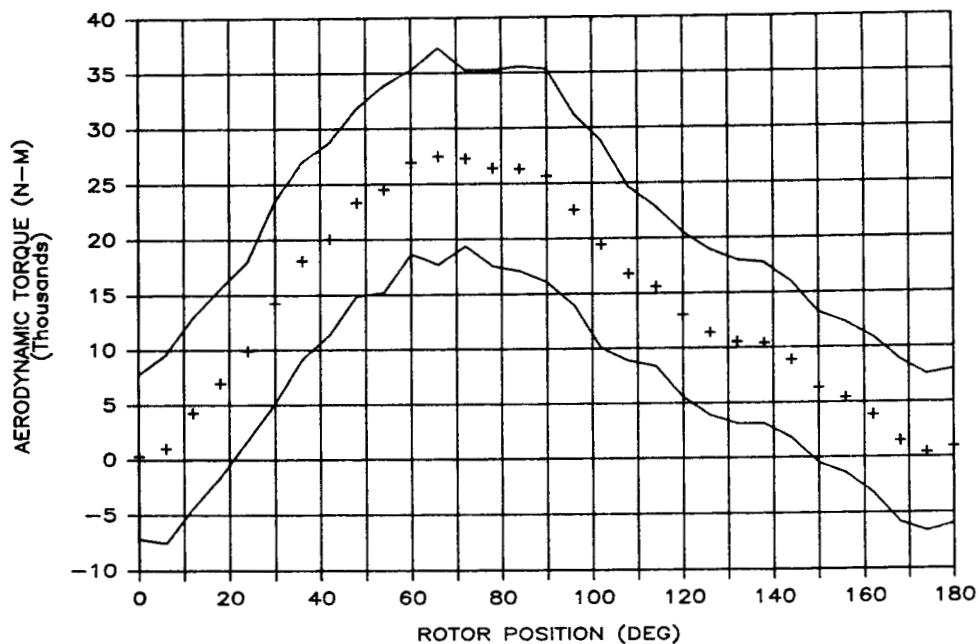


Figure 6. Standard deviations of aerodynamic torques in a bin, 50.6 rpm, TSR 2.87

50.6 RPM TSR 5.08

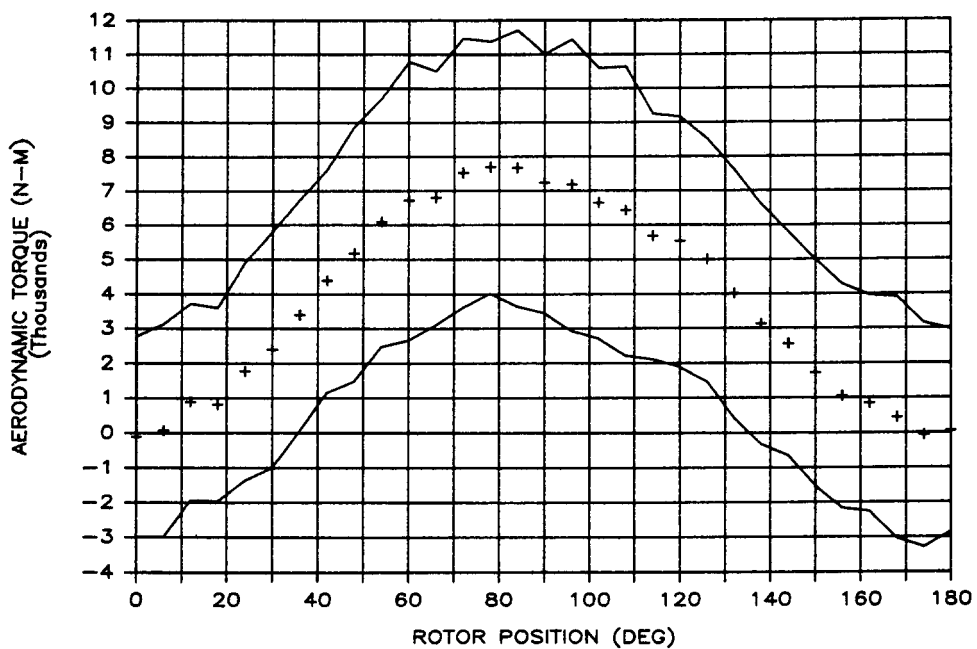


Figure 7. Standard deviations of aerodynamic torques in a bin, 50.6 rpm, TSR 5.08

## 4. Calculation of Aerodynamic Torque

Sandia National Laboratories currently uses a double-multiple stream-tube model known as SIDIF (for *S*Ine *D*istribution *I*nterference *F*actor) to calculate the torque and power produced by VAWTs. Double-multiple stream-tube (DMS) techniques model the turbine as a number of independent stream tubes, each of which is modeled as two actuator disks: one for the upwind passage of the turbine blade and a second for the downwind passage of the blade. Conservation of momentum is applied to each actuator disk to determine the time-averaged forces on the turbine blades. This technique yields quite accurate performance estimates and detailed blade loadings. The models separate the upwind and downwind blade loadings, in contrast to the single-multiple stream-tube models, which only yield the sum of the upwind and downwind blade loads for each stream tube. Although the DMS models yield significantly more information, the computation time is not much greater than for single-multiple stream-tube models.

### 4.1 SIDIF Model

The SIDIF code splits the turbine into a number of stream tubes rotationally (typically, into  $5^\circ$  increments) and vertically (typically, into 21 equal-height increments). It models the velocity decrease that occurs as the incident wind passes through the upwind or downwind section of the VAWT as a sinusoidal function with the maximum velocity decrement occurring at relative angles of  $90^\circ$  and  $270^\circ$  ( $0^\circ$  is defined as the reference blade pointing directly into the incident wind). This sinusoidal velocity decrement distribution specifies the relative velocity distribution (and thus the relative blade loadings) horizontally across the stream tubes. The model estimates a nominal upwind velocity decrement at a given height and calculates the resultant forces acting on the upwind section of the turbine at that height. It also calculates the change in momentum that occurs as the incident

wind passes through that upwind section of the turbine, and compares the change to the blade forces. If the two do not agree, a simple replacement iteration scheme determines the necessary velocity decrement (and, therefore, the blade loadings). A similar scheme determines the downstream velocity decrements and blade loadings. The blade loadings are integrated over the height of the turbine and are properly summed (to account for the number of turbine blades) to determine the rotationally resolved rotor loadings.

SIDIF incorporates the effects of the boundary layer of the incident wind, nonuniform velocity between the upwind and downwind sections of the rotor, dynamic stall effects, and local blade Reynolds number variations. More information on the code, including comparisons with experimental data, may be found in Berg,<sup>2</sup> who discusses a code called CODIF (for *C*O sine *D*istribution *I*nterference *F*actor). SIDIF is simply CODIF rewritten for a reference rotational angle that is rotated  $90^\circ$  with respect to the incident wind.

### 4.2 Dynamic Stall Model

Dynamic stall is present on VAWT blades during high wind-speed operation<sup>10,11</sup> and it must be included in the VAWT model if that model is to yield accurate results at maximum power conditions. The SIDIF code incorporates the Boeing-Vertol (or Gormont) model<sup>12</sup> developed for use on helicopters. In this method, the lift-coefficient hysteresis and drag-coefficient shift observed in dynamic stall experiments are approximated by combining static wind-tunnel airfoil-section data with an empirically derived stall-delay representation. This model has been modified as suggested by Massé<sup>13</sup> to cause the dynamic stall effects to diminish at large angles of attack, in agreement with experimental data. Berg discusses the implementation of this model in greater detail.<sup>2</sup>

## 5. Results

Data records obtained at each of the rotor operating speeds were reduced using the approach based on the Method of Bins and combined into a single set of data to obtain sufficient data to span the full operating range of the turbine. In what follows, data are presented for half a revolution of the rotor. This range is indicated in all plots and tables by relative rotor positions from  $0^\circ$  to  $180^\circ$ . A relative rotor position of  $0^\circ$  corresponds to the incident wind normal to the plane of the rotor with one of the blades heading directly upwind and the second blade heading directly downwind.

All results have been corrected to a common density of  $1.00 \text{ kg/m}^3$  ( $0.0625 \text{ lbm/ft}^3$ ), which was arbitrarily selected as the standard for the location of the test. Reynolds numbers for the two operating rpms are 960 000 for 38.7 rpm and 1 250 000 for 50.6 rpm. These Reynolds numbers are based on the chord and tip speed of the blade and are averages for a full rotation.

### 5.1 Results for 38.7 rpm

Because of the lower rotational speed, the results for this case yield more complete data at low tip-speed ratios (higher relative wind speed), in particular in the range 2.0 to 3.0. Figures 8 and 9 show the aerodynamic torque for 38.7 rpm (Reynolds number 960 000) for tip-speed ratios of 2.20 to 7.98. The spacing of the plotted data indicates the trends with increasing tip-speed ratio. The data at a tip-speed ratio of 2.20 show a peak at a relative rotor position of  $50^\circ$  and a second peak at a relative rotor position of  $125^\circ$ . As tip-speed ratio increases (free-stream velocity decreases), the maximum torque decreases, the location of the peak torque moves to the right toward  $90^\circ$ , and the secondary peak near  $120^\circ$  is no longer evident. The data shown in Figure 9 for tip-speed ratios of 3.89 to 7.98 continue to show similar trends. A different scale was used for the torque in these two figures and the results for a tip-speed ratio of 3.89 have been shown on each figure to allow us to compare the two sets of data. The data are presented in tabular form in Table 1 for all tip-speed ratios plotted. The  $C_p$  included at the bottom of each column is based on the rotationally averaged torque.

To illustrate the torque for low tip-speed ratios, data from each output bin were extracted. Figure 10

shows the results at tip-speed ratios of 2.02 and 2.08. These two curves are similar, with the peak at  $125^\circ$  evident in both. There is more scatter in these curves than in Figures 8 and 9 as the number of data values in each bin is smaller because of a lack of high-wind data. Additional data at increasing tip-speed ratios are shown in Figures 11 to 13. As the tip-speed ratio increases, the magnitude of the peak at  $125^\circ$  decreases, and there may be a slight shift of the peak to a smaller value of relative rotor position. In interpreting these data, it is important to remember that the results were sorted into bins  $6^\circ$  wide. The relative rotor position was also based on a wind direction measured above the rotor. At best, one could expect values to be accurate to within plus or minus one bin. The exact location of the secondary peak is therefore of less importance than its relative location and magnitude. This secondary peak has almost completely disappeared by a tip-speed ratio of 2.86 (Figure 8). This peak may be due to the presence of dynamic stall, a change in the lift and drag created on the airfoil due to unsteady effects, but these data are not extensive enough to conclusively support that hypothesis. Table 2 contains the data shown in Figures 10 through 13.

Comparisons between the measured aerodynamic torques and the predictions using the SIDIF double-multiple stream-tube model are shown in Figures 14 through 20. These data were computed in increments of 0.5 in tip-speed ratio and are presented as such. Measurements were selected that were closest in tip-speed ratio to the computed value. Because of the width of the bin used in sorting as a function of wind speed, the calculated value would fall into the corresponding measurement bin in each case. The routine used to plot the calculated values drew straight line segments between data points, and the discontinuities in slope in the predictions are due to this feature and not the SIDIF model. In considering these comparisons, the area under either of the curves is proportional to the output power of the rotor. If a comparison of measured and predicted power were made, only this area would be compared and the agreement would be quite good. Also, the scales on each plot were selected to fill the grid, and at the larger tip-speed ratios (lower torques) the apparent large differences are only accentuated by the choice of scale.

38.7 RPM

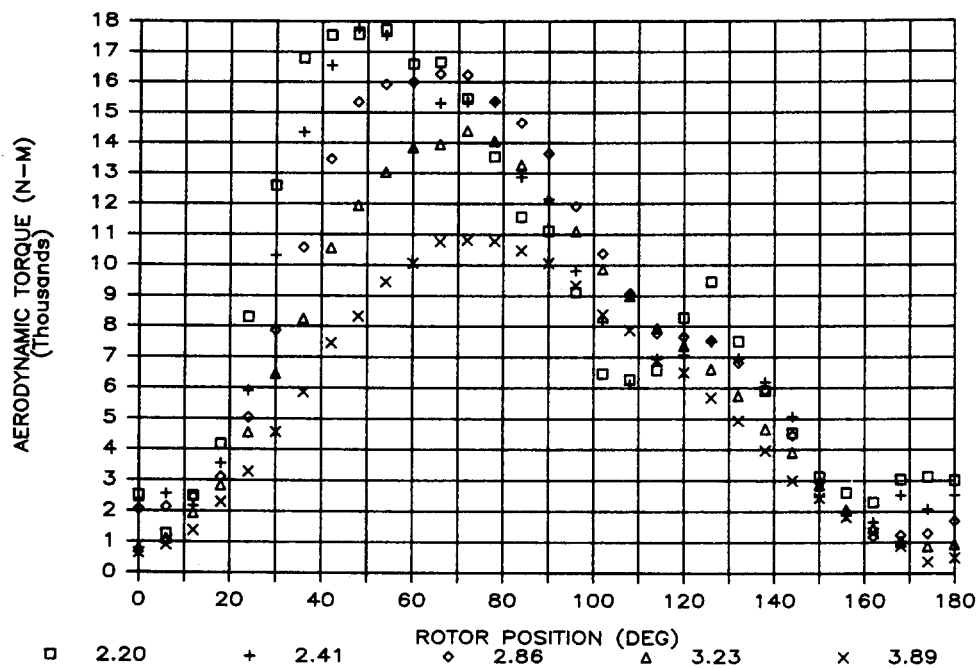


Figure 8. Aerodynamic torque as a function of tip-speed ratio, 38.7 rpm, TSR 2.20 to 3.89

38.7 RPM

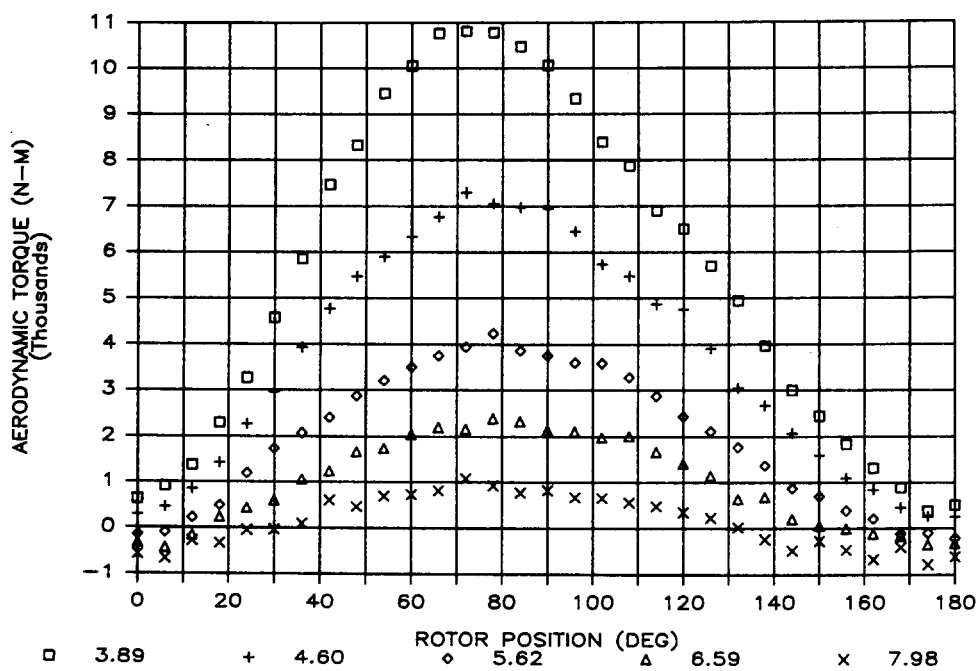
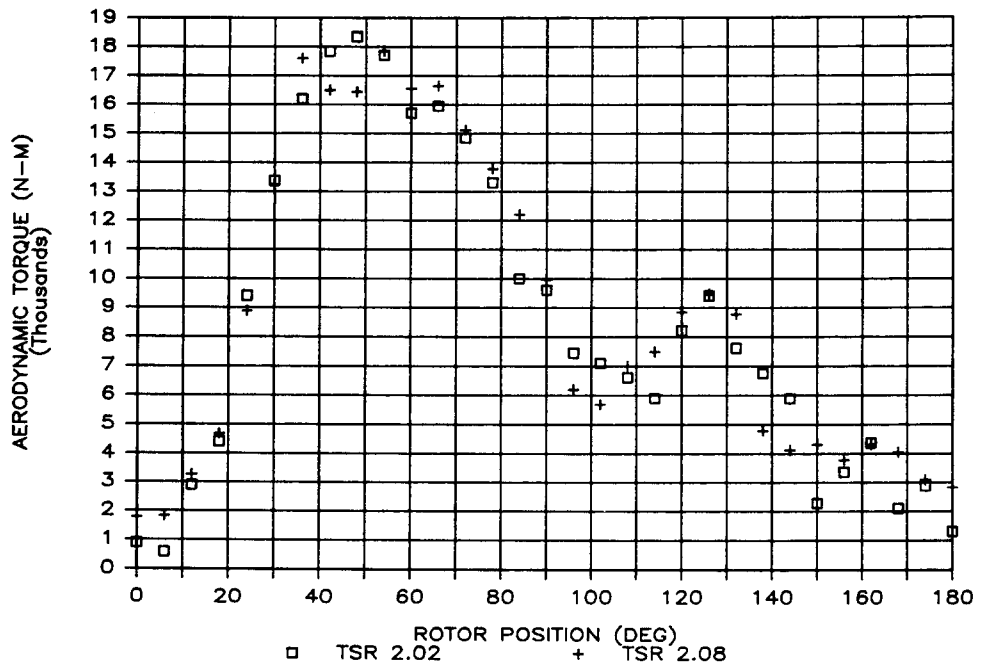


Figure 9. Aerodynamic torque as a function of tip-speed ratio, 38.7 rpm, TSR 3.89 to 7.98

**Table 1. Aerodynamic torques in N-M, 38.7 rpm** (Data correspond to Figures 8 and 9)

Relative Rotor Position	Tip-Speed Ratio								
	2.20	2.41	2.86	3.23	3.89	4.60	5.62	6.59	7.98
0	2530	2318	2058	812	641	288	-144	-317	-577
6	1267	2555	2135	1098	913	455	-97	-433	-664
12	2493	2160	2454	1937	1375	857	222	-159	-278
18	4189	3549	3104	2842	2297	1427	489	235	-334
24	8312	5920	5050	4561	3272	2273	1201	438	-52
30	12597	10319	7881	6458	4574	2962	1729	601	-35
36	16803	14364	10580	8249	5865	3933	2075	1064	95
42	17554	16564	13471	10566	7465	4773	2414	1248	604
48	17574	17785	15347	11952	8332	5469	2879	1663	464
54	17752	17542	15924	13036	9458	5907	3212	1740	698
60	16604	15992	16008	13848	10058	6344	3504	2044	733
66	16663	15315	16269	13954	10761	6774	3755	2201	821
72	15464	15365	16239	14398	10810	7298	3941	2159	1085
78	13543	15351	15374	14059	10777	7054	4232	2388	931
84	11565	12873	14658	13264	10472	6972	3861	2323	776
90	11115	12156	13638	12143	10061	6948	3754	2132	825
96	9114	9805	11913	11107	9334	6453	3600	2107	675
102	6474	8158	10377	9863	8392	5733	3585	1983	661
108	6286	6126	9076	8990	7874	5473	3280	2008	559
114	6593	6957	7781	7949	6898	4868	2874	1664	479
120	8295	7086	7665	7383	6509	4758	2432	1415	345
126	9469	7516	7542	6623	5696	3910	2116	1146	229
132	7520	6963	6830	5757	4941	3055	1764	638	16
138	5911	6203	5934	4670	3970	2675	1363	681	-239
144	4554	5078	4467	3909	3004	2076	874	201	-481
150	3132	2512	2951	2867	2447	1596	695	55	-274
156	2624	1888	1970	2066	1832	1087	380	-12	-469
162	2308	1666	1195	1477	1310	843	210	-120	-675
168	3044	2540	1238	1032	890	449	-118	-166	-407
174	3124	2075	1291	884	373	251	-103	-356	-785
180	3022	2536	1696	939	505	246	-217	-327	-616
$C_p$	0.040	0.132	0.217	0.272	0.373	0.409	0.395	0.325	0.089

### 38.7 RPM



**Figure 10.** Aerodynamic torque as a function of tip-speed ratio, 38.7 rpm, TSR 2.02 and 2.08

### 38.7 RPM

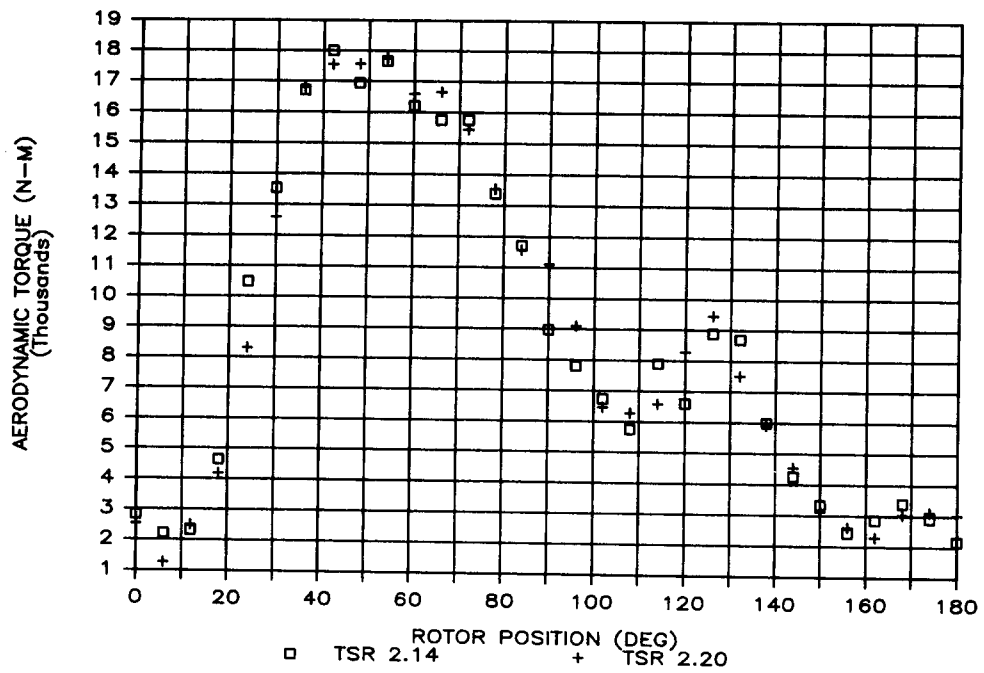


**Figure 11.** Aerodynamic torque as a function of tip-speed ratio, 38.7 rpm, TSR 2.14 and 2.20

38.7 RPM

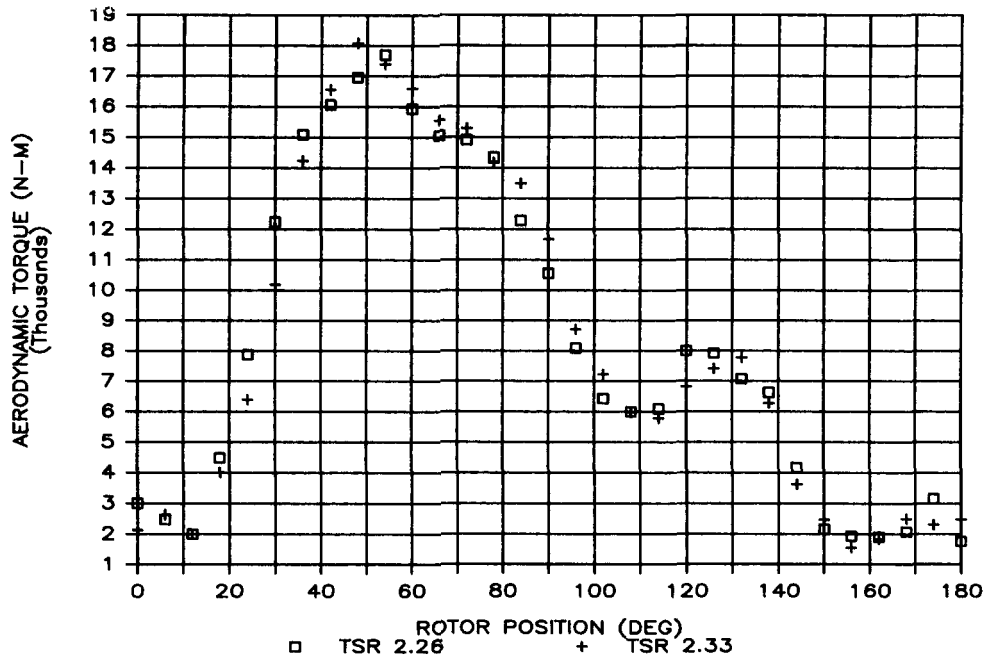


Figure 12. Aerodynamic torque as a function of tip-speed ratio, 38.7 rpm, TSR 2.26 and 2.33

38.7 RPM

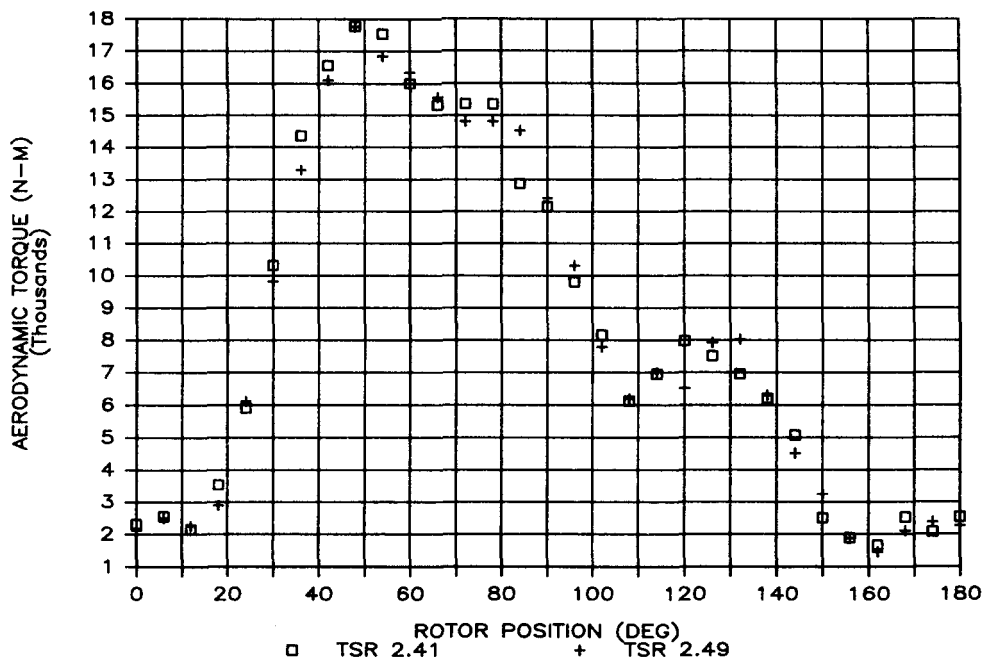
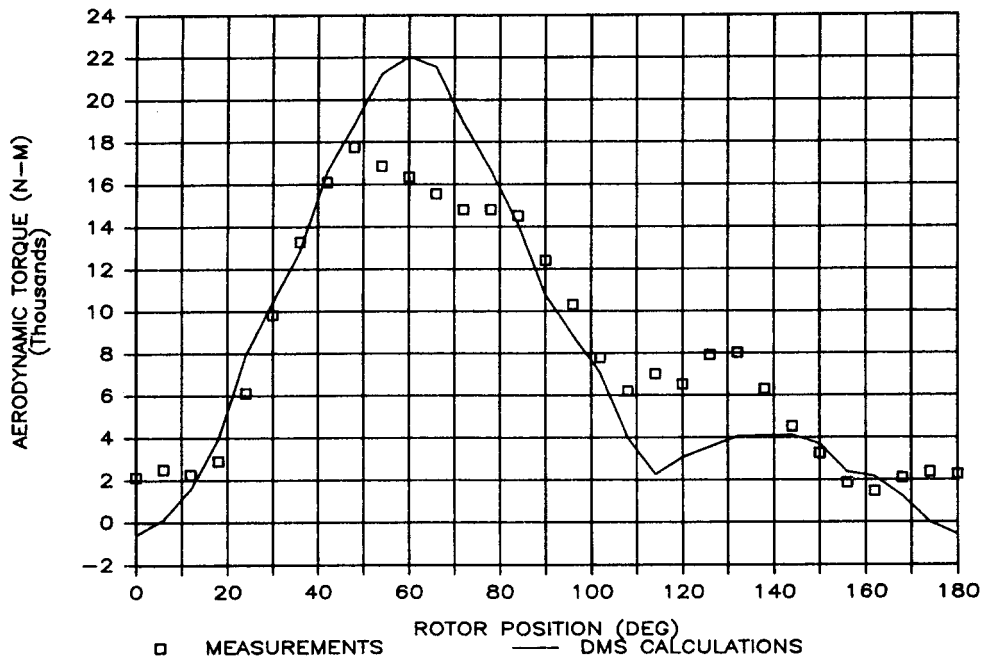


Figure 13. Aerodynamic torque as a function of tip-speed ratio, 38.7 rpm, TSR 2.41 and 2.49

**Table 2. Aerodynamic torques in N-M, 38.7 rpm** (Data for low tip-speed ratios presented in Figures 10 to 13)

Relative Rotor Position	Tip-Speed Ratio							
	2.02	2.08	2.14	2.20	2.26	2.33	2.41	2.49
0	886	1767	2829	2530	3003	2129	2318	2131
6	577	1827	2213	1267	2477	2643	2555	2507
12	2908	3263	2314	2492	2003	1997	2160	2258
18	4408	4674	4637	4189	4487	4011	3549	2901
24	9418	8892	10488	8312	7886	6402	5920	6119
30	13380	13260	13536	12597	12240	10197	10319	9829
36	16204	17611	16719	16803	15092	14244	14364	13305
42	17857	16498	18012	17554	16066	16565	16564	16109
48	18351	16454	16948	17574	16971	18092	17785	17757
54	17713	17856	17661	17752	17707	17401	17542	16858
60	15700	16551	16204	16604	15938	16602	15992	16349
66	15948	16652	15758	16663	15055	15557	15315	15556
72	14845	15122	15761	15464	14915	15297	15365	14810
78	13313	13781	13384	13543	14358	14181	15351	14814
84	10001	12217	11704	11565	12284	13495	12873	14527
90	9612	9969	8976	11115	10557	11677	12156	12424
96	7449	6203	7809	9114	8095	8711	9805	10313
102	7097	5689	6744	6474	6430	7226	8158	7793
108	6609	7015	5751	6286	5997	5972	6126	6197
114	5907	7490	7904	6593	6099	5780	6957	7006
120	8219	8845	6617	8295	8012	6825	7986	6518
126	9412	9471	8889	9469	7930	7419	7516	7925
132	7615	8769	8703	7520	7080	7781	6963	8026
138	6743	4779	5991	5911	6630	6277	6203	6298
144	5889	4121	4254	4554	4164	3630	5078	4523
150	2286	4298	3342	3132	2160	2475	2513	3257
156	3364	3780	2433	2624	1928	1544	1888	1874
162	4365	4314	2863	2308	1903	1823	1666	1456
168	2103	4049	3408	3044	2071	2505	2540	2107
174	2883	3095	2924	3124	3162	2317	2075	2381
180	1301	2839	2178	3022	1757	2491	2536	2258

### 38.7 RPM TSR 2.5



**Figure 14.** Comparison between measured and predicted aerodynamic torque, 38.7 rpm, TSR 2.5

### 38.7 RPM TSR 3.0

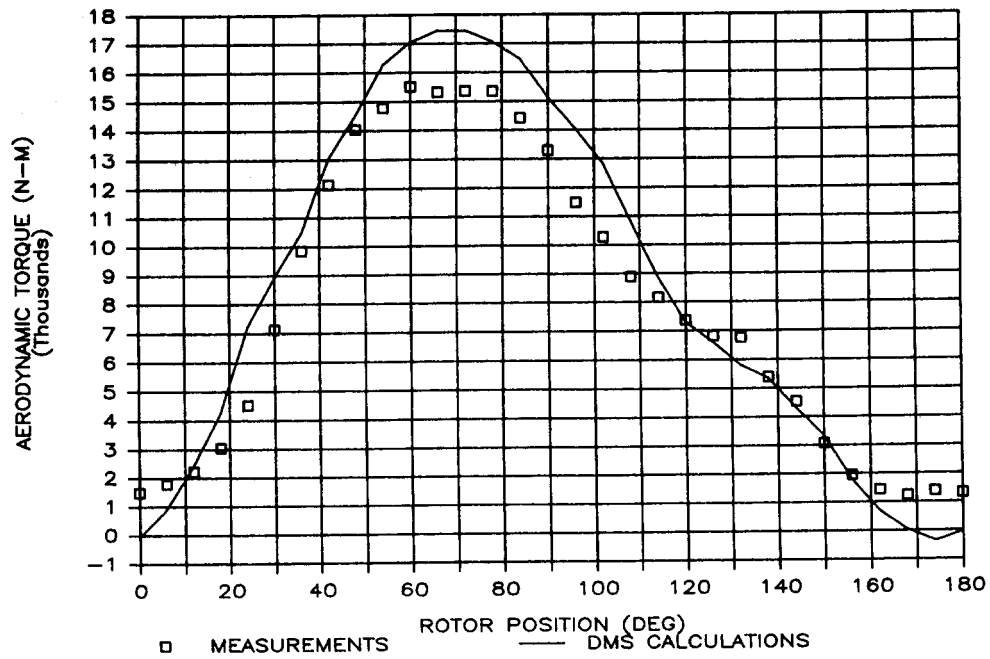


**Figure 15.** Comparison between measured and predicted aerodynamic torque, 38.7 rpm, TSR 3.0

### 38.7 RPM TSR 3.5

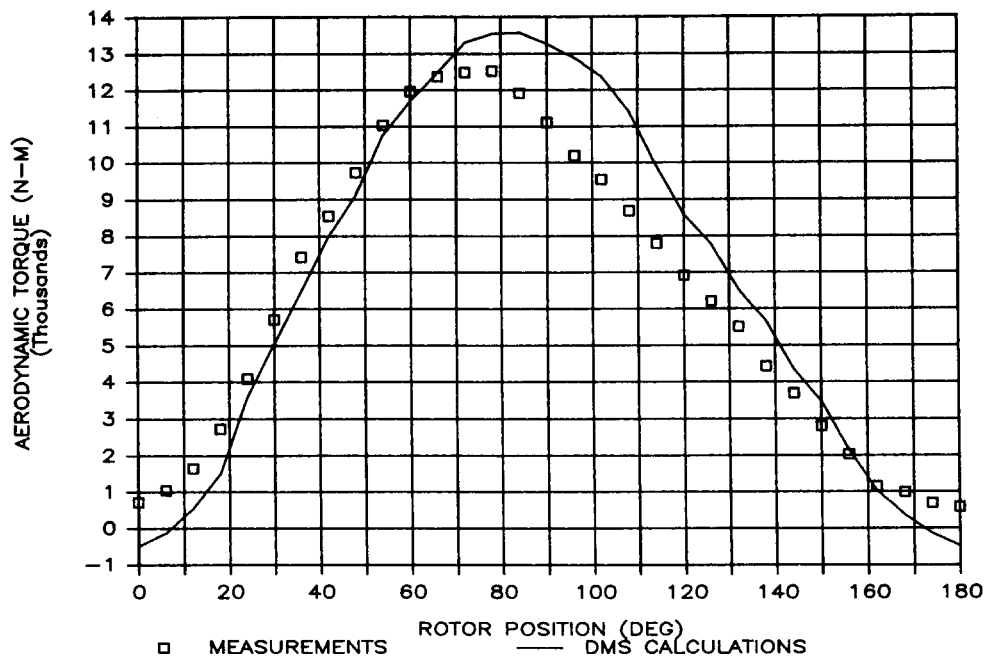


**Figure 16.** Comparison between measured and predicted aerodynamic torque, 38.7 rpm, TSR 3.5

### 38.7 RPM TSR 4.0

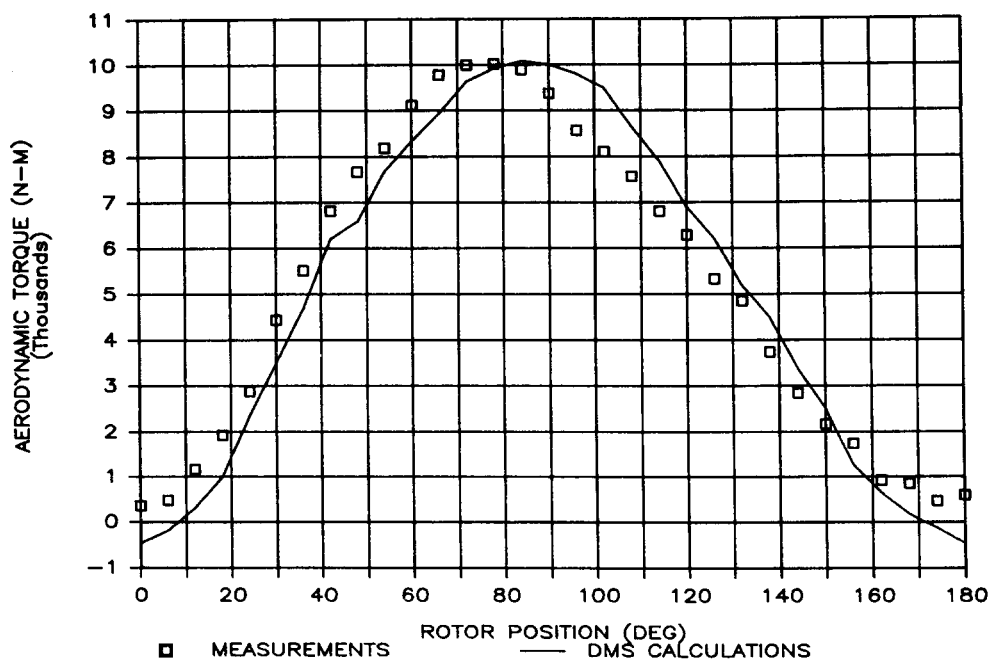


**Figure 17.** Comparison between measured and predicted aerodynamic torque, 38.7 rpm, TSR 4.0

### 38.7 RPM TSR 4.5

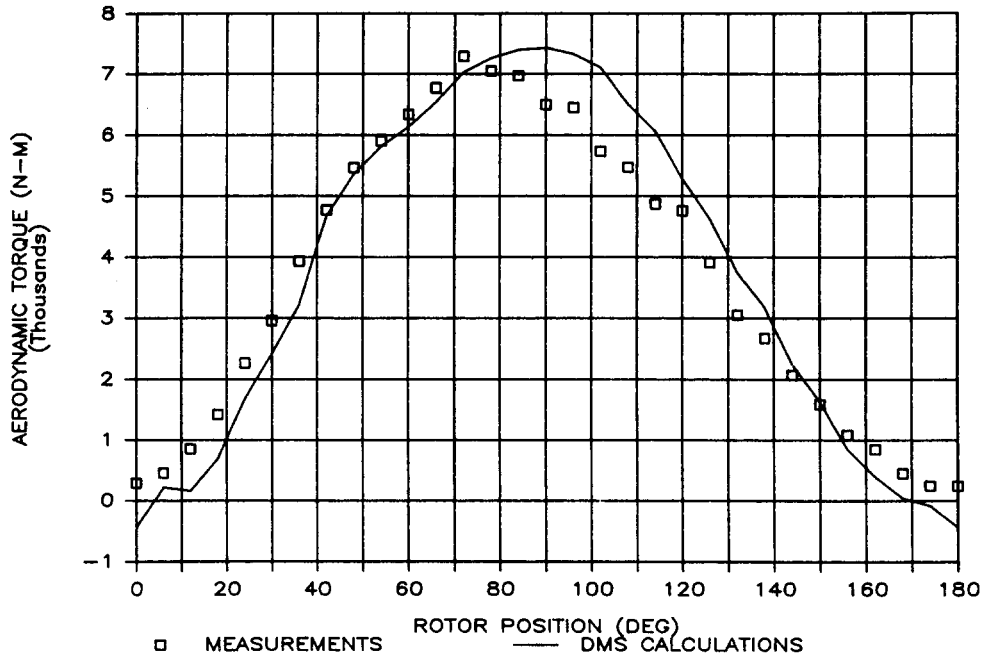


Figure 18. Comparison between measured and predicted aerodynamic torque, 38.7 rpm, TSR 4.5

### 38.7 RPM TSR 5.5

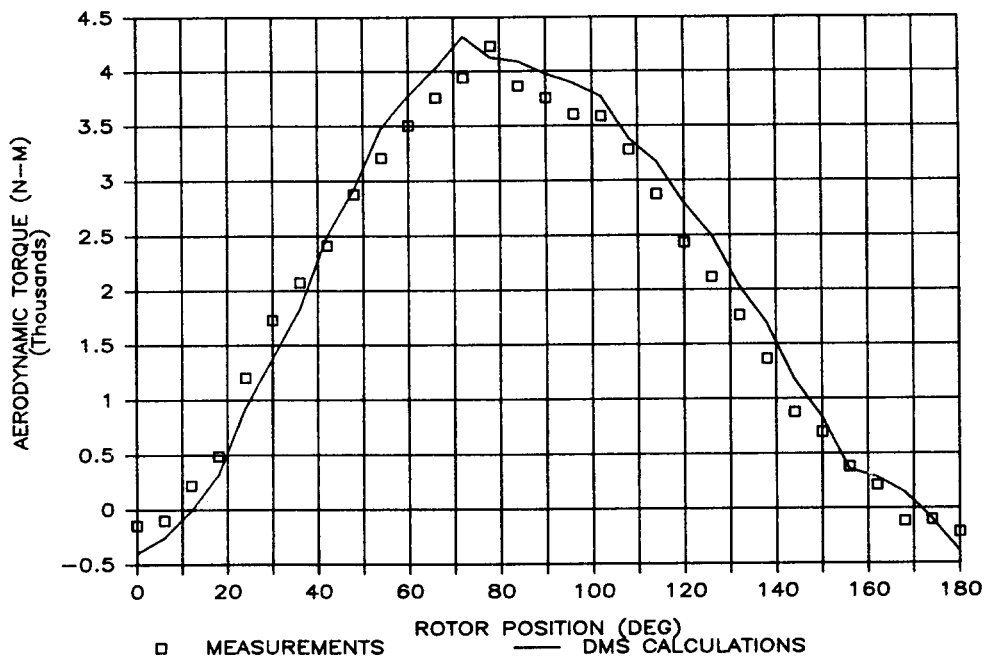
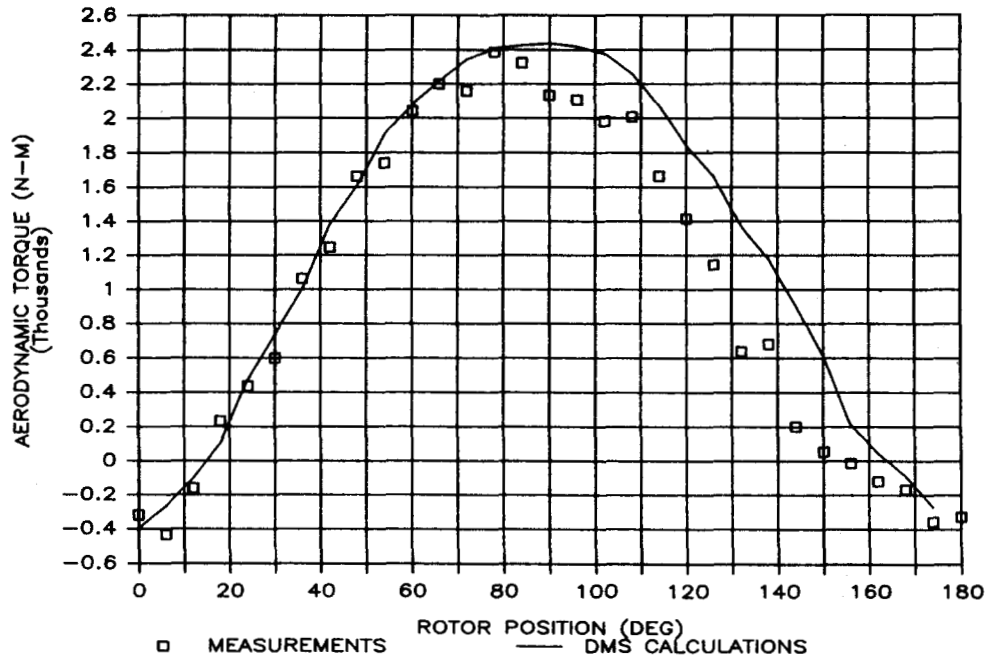


Figure 19. Comparison between measured and predicted aerodynamic torque, 38.7 rpm, TSR 5.5

## 38.7 RPM TSR 6.5



**Figure 20.** Comparison between measured and predicted aerodynamic torque, 38.7 rpm, TSR 6.5

The data for a tip-speed ratio of 2.5 shown in Figure 14 exhibit a tendency of the model to overpredict the torque at relative rotor positions of 60° to 80°, and to underpredict the torque from 110° to 150°. These differences are probably due to the choice of the dynamic-stall model in the double-multiple stream-tube model. These differences are less evident at a tip-speed ratio of 3.0 (Figure 15) and continue to decrease up to a tip-speed ratio of 5.5 (Figure 19). For these higher tip-speed ratios, the agreement between the measurements and predictions is excellent. Some of the differences evident for relative rotor positions between 90° and 150° may be due to the difficulties associated with the measurement of the rotor position. The only significant differences in this series of comparisons are for the low tip-speed ratios where dynamic stall seems to be a factor.

## 5.2 Results for 50.6 rpm

A summary of the results for 50.6 rpm (Reynolds number 1 250 000) is shown in Figures 21 and 22 for tip-speed ratios of 2.87 to 7.93. These data are listed in Table 3. They are similar to those for 38.7 rpm except there is less evidence of the secondary peak near a relative rotor position of 120°. This difference could be caused by the lack of data at the lower tip-speed ratios for this rpm.

The comparisons between the measurements and the calculations using the double-multiple stream-tube model are shown in Figures 23 through 29. The differences at a tip-speed ratio of 2.5 are very similar to those for 38.7 rpm (Figure 14). The measurements are less than the predictions in the range of relative rotor positions of 40° to 90°, and the measurements are greater than the predictions in the range of 110° to 150°. For all higher tip-speed ratios, the agreement is good. At the highest tip-speed ratios, 6.5 and 7.5, the differences between the measurements and calculations are of the order of the accuracy of the measurements.

### 50.6 RPM

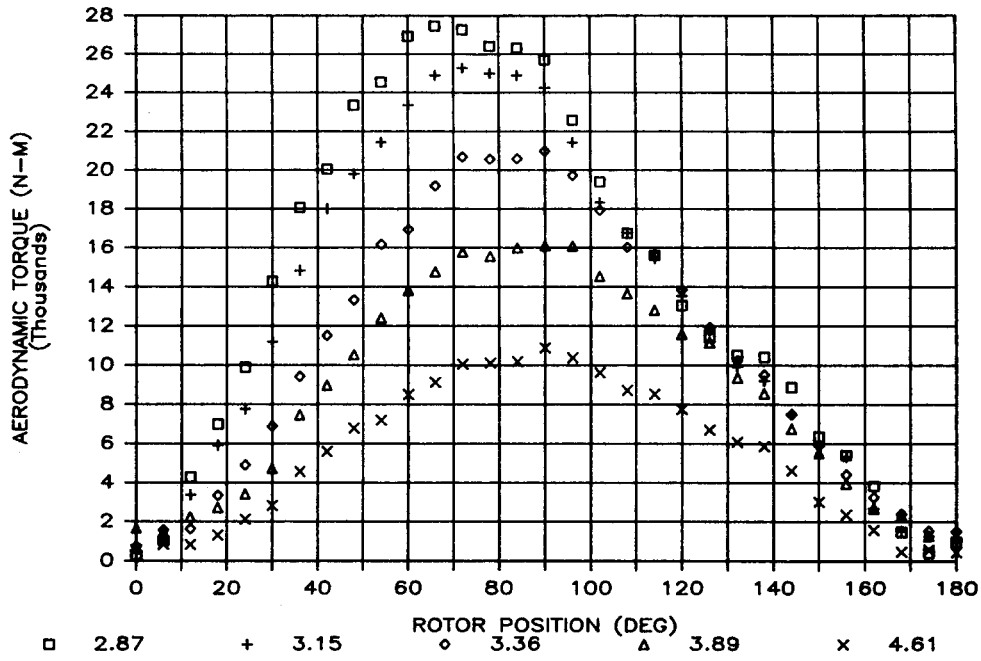


Figure 21. Aerodynamic torque as a function of tip-speed ratio, 50.6 rpm, TSR 2.87 to 4.61

### 50.6 RPM

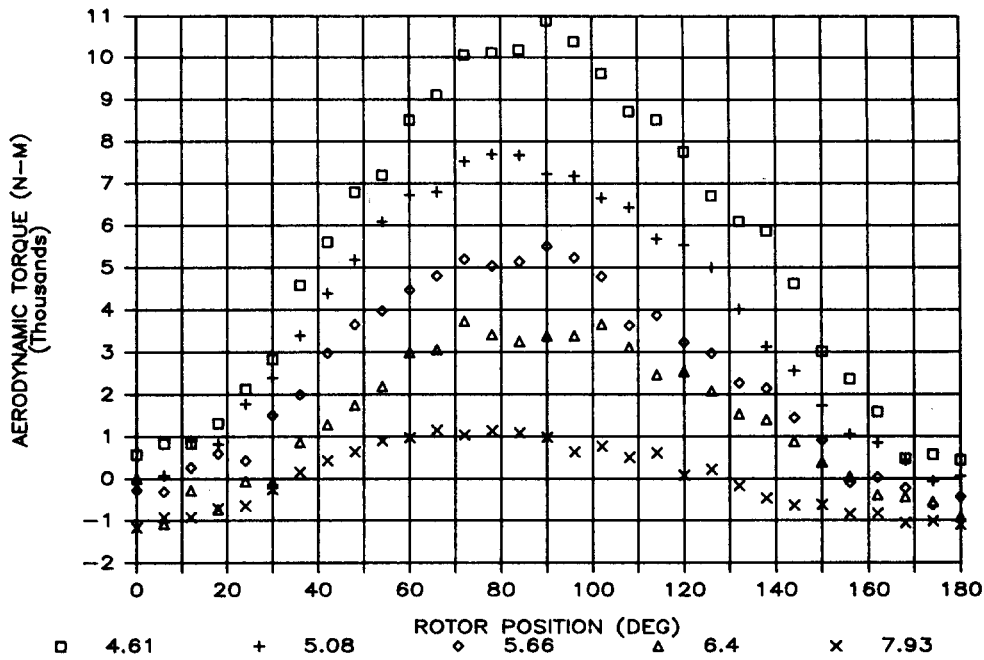
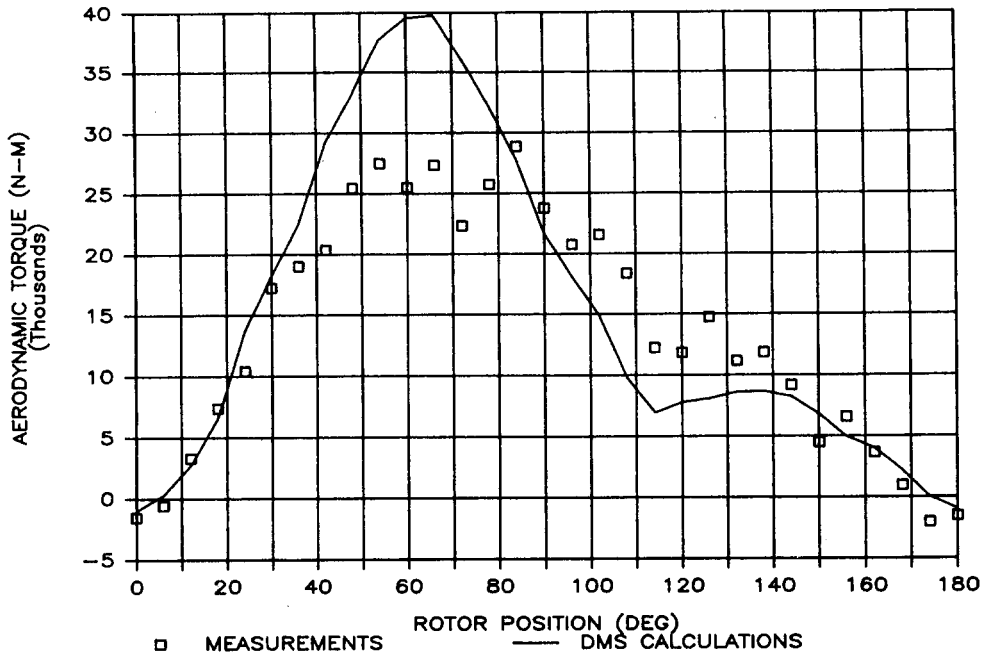


Figure 22. Aerodynamic torque as a function of tip-speed ratio, 50.6 rpm, TSR 4.61 to 7.93

**Table 3. Aerodynamic torques in N-M, 50.6 rpm** (Data correspond to Figures 21 and 22)

Relative Rotor Position	Tip-Speed Ratio								
	2.87	3.15	3.36	3.89	4.61	5.08	5.66	6.40	7.93
0	303	753	1107	1673	571	-107	-276	-1083	-1165
6	1043	1032	1327	1416	836	72	-312	-283	-926
12	4302	3381	2628	2248	832	898	267	-736	-917
18	6995	5921	4560	2724	1317	822	590	-65	-716
24	9902	7775	6128	3409	2125	1778	427	-102	-652
30	14277	11204	9228	4727	2838	2400	1506	866	-254
36	18077	14840	11647	7466	4585	3395	1996	1285	157
42	20054	18014	13863	8973	5607	4393	2982	1743	433
48	23336	19810	16006	10535	6795	5184	3651	2194	645
54	24533	21444	18347	12396	7201	6095	3982	2994	902
60	26929	23342	20146	13788	8516	6725	4474	3064	971
66	27465	24885	22189	14763	9116	6803	4806	3730	1158
72	27284	25285	22217	15780	10064	7534	5198	3412	1038
78	26412	24996	22357	15561	10119	7699	5043	3248	1138
84	26310	24880	22537	15993	10186	7674	5146	3384	1087
90	25686	24239	21236	16115	10889	7232	5509	3393	977
96	22576	21417	20433	16086	10388	7178	5235	3657	640
102	19402	18344	18467	14537	9624	6655	4790	3119	769
108	16756	16762	16944	13645	8722	6430	3630	2472	508
114	15602	15445	15398	12797	8523	5684	3869	2541	614
120	13039	13523	13997	11577	7760	5536	3226	2079	81
126	11410	11770	12084	11148	6704	5003	2970	1538	221
132	10528	9923	10642	9349	6092	4015	2271	1394	-165
138	10407	9199	9152	8563	5866	3127	2141	876	-467
144	8872	7492	7218	6766	4625	2566	1449	390	-634
150	6349	5896	5681	5528	3016	1732	905	48	-619
156	5417	5336	4477	3946	2367	1056	-97	-391	-839
162	3838	2685	3145	2683	1585	845	31	-435	-822
168	1484	1539	1303	2302	473	432	-224	-552	-1057
174	416	1276	1085	1275	571	-66	-625	-919	-1016
180	968	710	1623	1196	437	57	-439	-726	-1099
$C_p$	0.220	0.267	0.293	0.342	0.357	0.338	0.293	0.244	0.012

### 50.6 RPM TSR 2.5



**Figure 23.** Comparison between measured and predicted aerodynamic torque, 50.6 rpm, TSR 2.5

### 50.6 RPM TSR 3.0

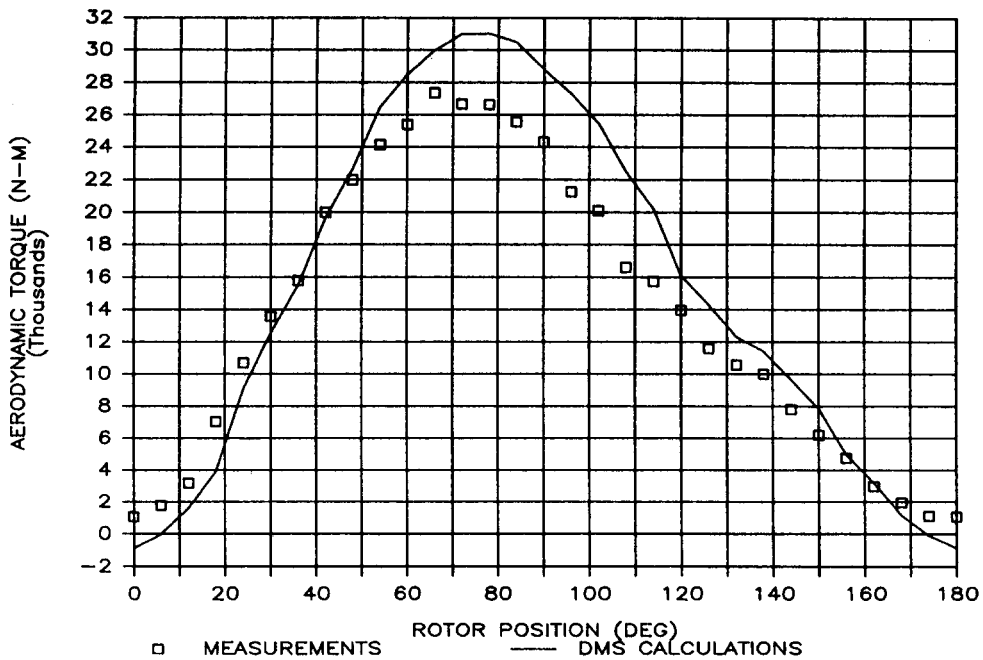


**Figure 24.** Comparison between measured and predicted aerodynamic torque, 50.6 rpm, TSR 3.0

### 50.6 RPM TSR 3.5

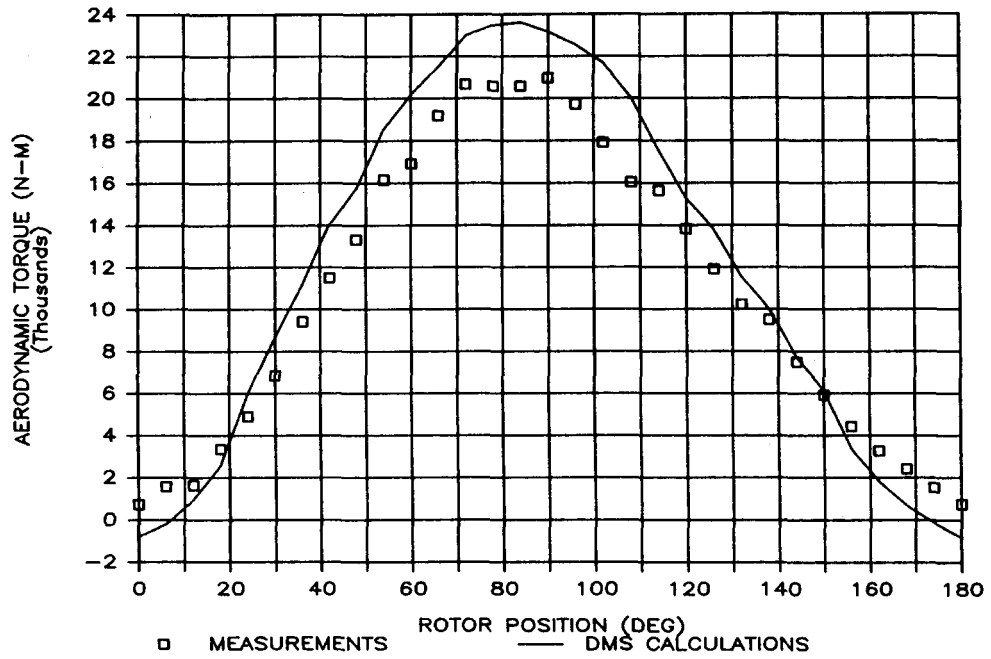


Figure 25. Comparison between measured and predicted aerodynamic torque, 50.6 rpm, TSR 3.5

### 50.6 RPM TSR 4.0

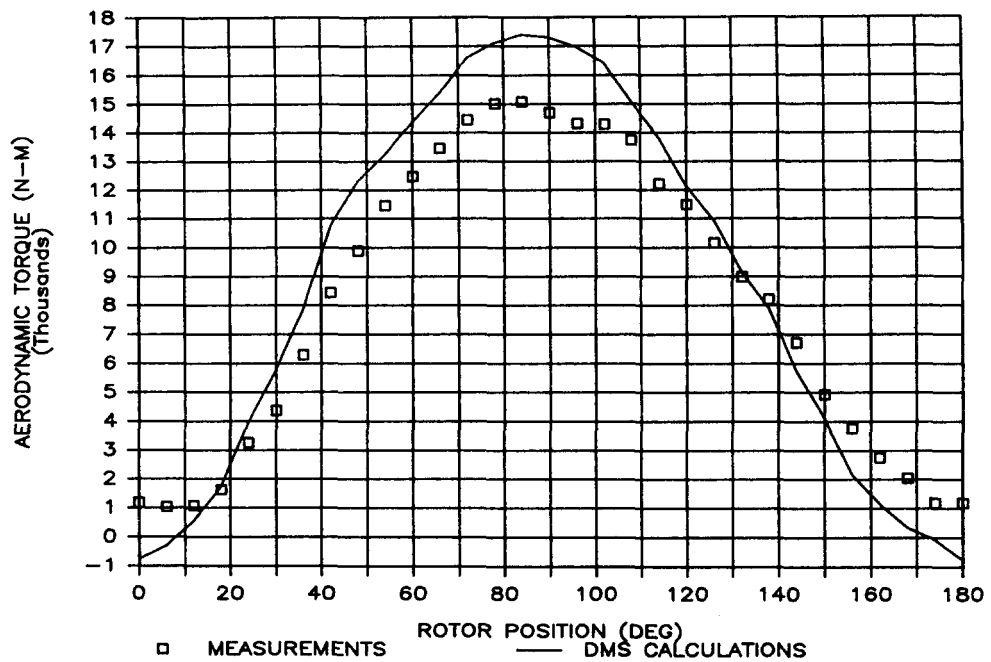


Figure 26. Comparison between measured and predicted aerodynamic torque, 50.6 rpm, TSR 4.0

### 50.6 RPM TSR 4.5

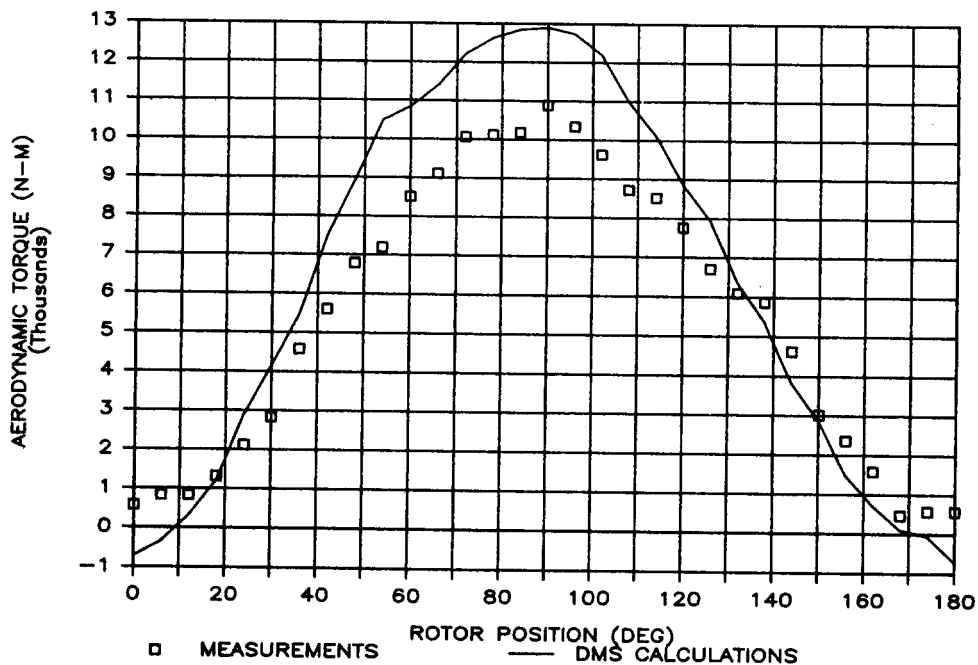


Figure 27. Comparison between measured and predicted aerodynamic torque, 50.6 rpm, TSR 4.5

### 50.6 RPM TSR 5.5

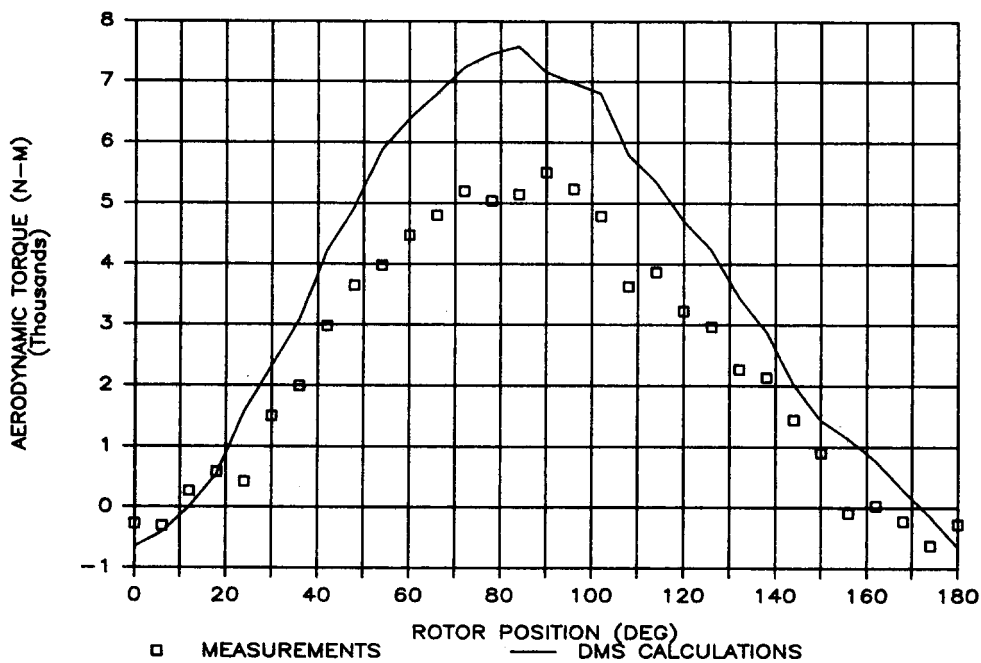


Figure 28. Comparison between measured and predicted aerodynamic torque, 50.6 rpm, TSR 5.5

50.6 RPM TSR 6.5

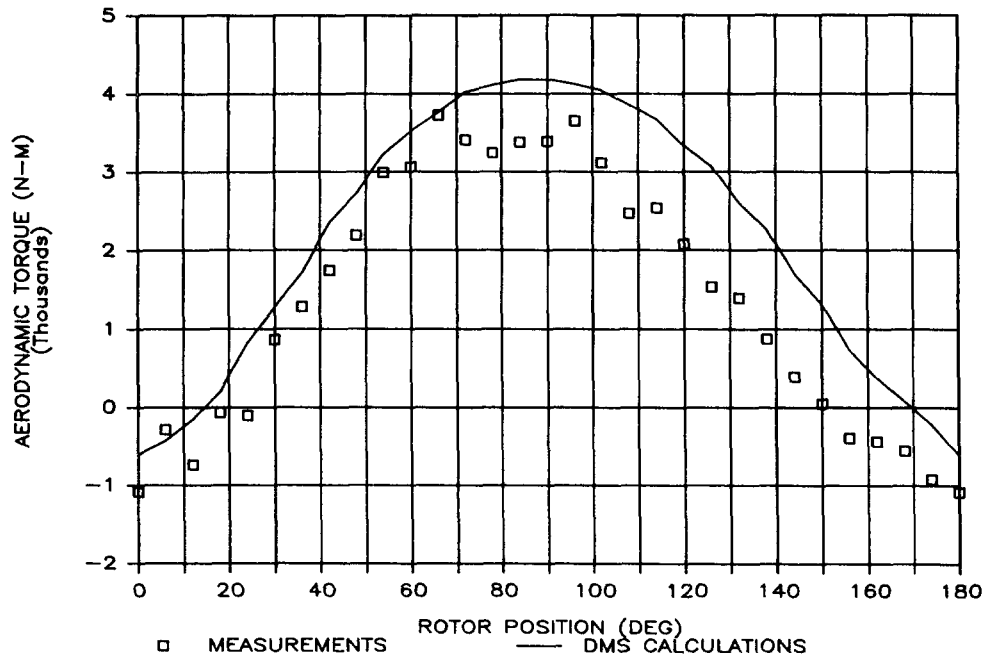


Figure 29. Comparison between measured and predicted aerodynamic torque, 50.6 rpm, TSR 6.5

### 5.3 Fourier Coefficients

The frequency content of the torque signatures is important in the structural analysis of the wind turbine. The forced periodicity of the data (it must repeat every 180°) results in Fourier coefficients at only even multiples of the rotation rate of the turbine. The Fourier coefficients of all torques were computed and normalized with the mean value of the torque. These coefficients are listed in Table 4 for the 38.7-rpm data

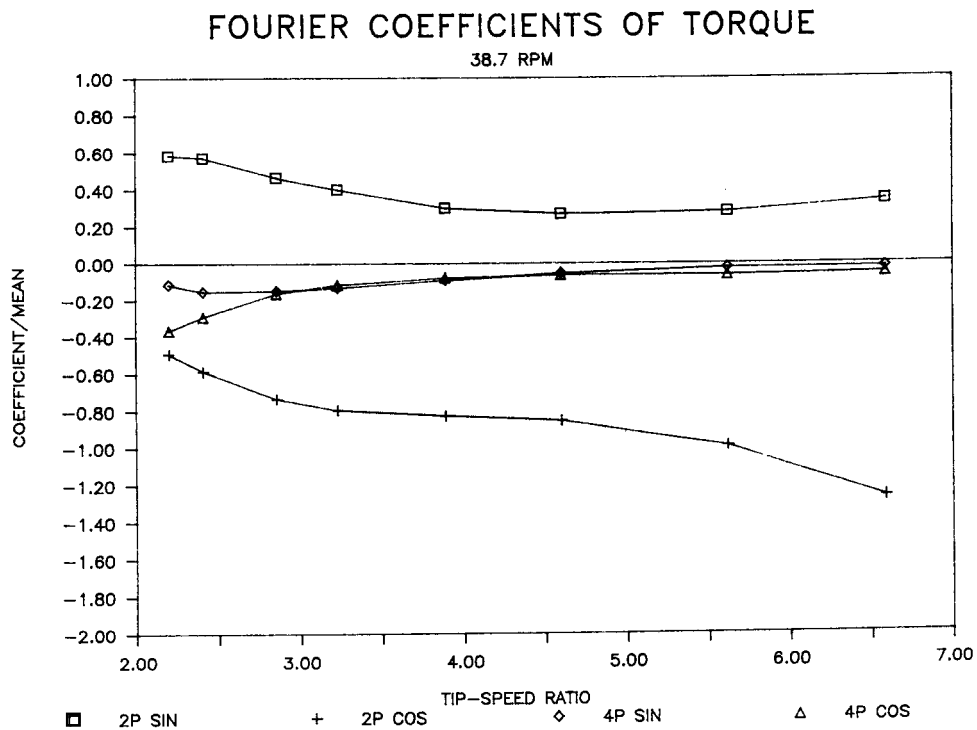
and Table 5 for the 50.6 rpm data. Coefficients are listed up to a frequency of 8P, where P is the rotation rate of the turbine. The coefficients for 2P and 4P are shown in Figures 30 and 31. The coefficients at 4P decrease in magnitude and the 2P coefficients become dominant with increasing tip-speed ratio. The cosine coefficient is much larger than the sine coefficient at high tip-speed ratios. The torque is closely approximated by a cosine curve with a mean value and a period half that of the turbine rotation.

Table 4. Fourier coefficients of torque, 38.7 rpm (Coefficients normalized with mean torque)

	Tip-Speed Ratio							
	2.20	2.41	2.86	3.23	3.89	4.60	5.62	6.59
0P SIN	0.00	0.00	0.00	0.00	0.00	0.00	0.00	0.00
0P COS	1.00	1.00	1.00	1.00	1.00	1.00	1.00	1.00
2P SIN	0.59	0.57	0.47	0.40	0.30	0.27	0.28	0.34
2P COS	-0.49	-0.59	-0.74	-0.80	-0.83	-0.85	-0.99	-1.27
4P SIN	-0.11	-0.15	-0.15	-0.13	-0.09	-0.05	-0.02	-0.02
4P COS	-0.37	-0.29	-0.16	-0.12	-0.08	-0.06	-0.07	-0.05
6P SIN	-0.05	-0.04	-0.00	-0.00	-0.00	-0.01	-0.01	-0.06
6P COS	0.02	0.02	0.03	0.01	0.01	-0.00	-0.02	0.01
8P SIN	-0.15	-0.09	-0.01	-0.02	-0.01	-0.02	-0.03	-0.03
8P COS	0.08	0.14	0.09	0.02	0.01	0.00	-0.02	-0.05

**Table 5. Fourier coefficients of torque, 50.6 rpm (Coefficients normalized with mean torque)**

	Tip-Speed Ratio							
	2.87	3.15	3.36	3.89	4.61	5.08	5.66	6.40
0P SIN	0.00	0.00	0.00	0.00	0.00	0.00	0.00	0.00
0P COS	1.00	1.00	1.00	1.00	1.00	1.00	1.00	1.00
2P SIN	0.41	0.35	0.23	0.06	0.03	0.15	0.21	0.34
2P COS	-0.78	-0.82	-0.85	-0.82	-0.89	-0.94	-1.12	-1.51
4P SIN	-0.13	-0.12	-0.01	-0.06	-0.04	-0.04	-0.05	-0.08
4P COS	-0.13	-0.08	-0.06	-0.04	-0.04	-0.07	-0.05	-0.10
6P SIN	0.00	0.00	0.01	0.01	0.05	0.01	0.02	-0.03
6P COS	-0.07	-0.05	-0.02	0.01	-0.02	0.02	-0.01	-0.04
8P SIN	0.00	-0.01	-0.00	0.01	0.01	-0.01	0.03	0.04
8P COS	0.00	0.01	-0.01	0.02	0.04	0.00	0.06	0.01



**Figure 30.** Fourier coefficients of torque, 38.7 rpm. These coefficients are normalized with the mean torque.

# FOURIER COEFFICIENTS OF TORQUE

50.6 RPM

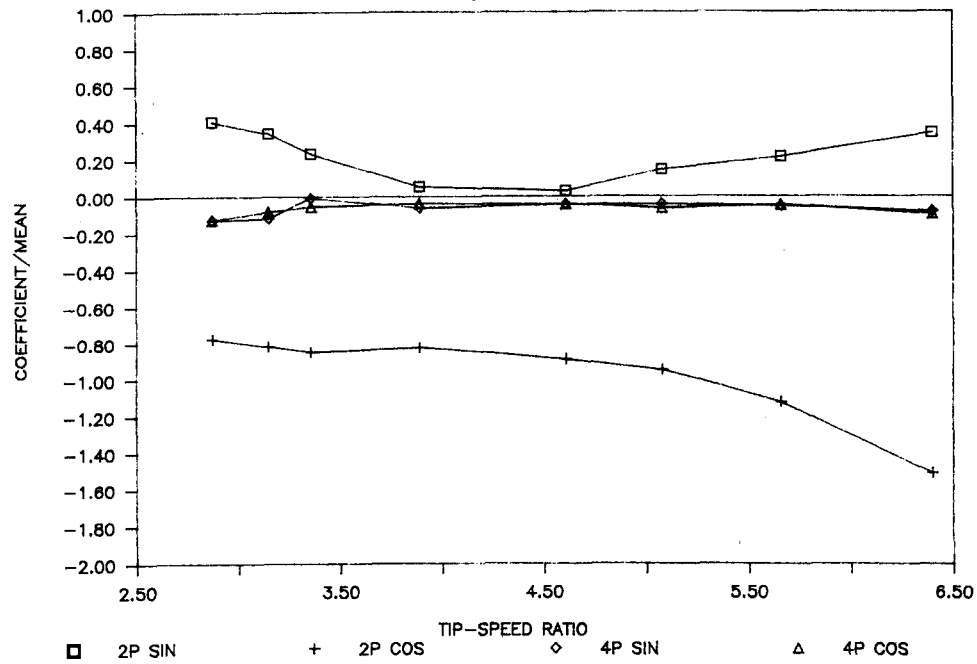


**Figure 31.** Fourier coefficients of torque, 50.6 rpm. These coefficients are normalized with the mean torque.

## 6. Conclusions

Measurements of low-speed torque and tangential acceleration at the turbine equator were used to determine the torque on a VAWT blade as a function of angle of rotation for a wide range of tip-speed ratios.

At low wind speeds (high tip-speed ratios), the torque is closely approximated by a cosine curve with a rotational period half that of the rotor itself. As the tip-speed ratio decreases (wind speed increases), the torque curve assumes a skewed character and the peak shifts from  $90^\circ$  toward  $50^\circ$ . At a tip-speed ratio of  $\sim 2.9$ , a secondary peak appears near  $125^\circ$ . This secondary peak grows in size as the tip-speed ratio drops further.

Comparisons of these experimentally determined torques with those calculated with the SIDIF code indicate that although the code does a good job of predicting the power over a wide range of tip-speed ratios, it does not accurately predict the rotationally resolved torque at lower tip-speed ratios—it over-

predicts the torque for relative rotor positions between  $50^\circ$  and  $90^\circ$  (the primary torque peak) and underpredicts the torque between  $110^\circ$  and  $150^\circ$  (the secondary torque peak). This results in errors in the frequency content and magnitude of the predicted loads, and thus inaccuracies in structural dynamic analyses of the turbine.

The major restrictions in the accuracy of the torques determined in this study were the assumption of rigid-body motion and the uncertainty in turbine rotational position. Additional studies to measure VAWT blade torque more accurately would be helpful in determining what areas of the aerodynamic load models are in error. Direct measurements of lift and drag (or their resultant torque) on a small blade section would be useful in this effort, because comparing observed and predicted values of lift and drag (or torque) over an entire blade tends to obscure the source of any observed differences.

## References

- <sup>1</sup>G. M. McNerney, *Accelerometer Measurements of Aerodynamic Torque on the DOE/Sandia 17-m Vertical-Axis Wind Turbine*, SAND80-2776 (Albuquerque, NM: Sandia National Laboratories, 1981).
- <sup>2</sup>D. E. Berg, "An Improved Double-Multiple Stream-tube Model for the Darrieus-Type Vertical-Axis Wind Turbine," *Proceedings of Sixth Biennial Wind Energy Conference* (Minneapolis, MN: American Solar Energy Society, June 1983).
- <sup>3</sup>I. Paraschivoiu, "Aerodynamic Loads and Performance of the Darrieus Rotor," *AIAA Journal of Energy*, 6(6)(1982).
- <sup>4</sup>F. Johnston, Jr., ed, *Proceedings of the Vertical-Axis Wind Turbine (VAWT) Design Technology Seminar for Industry*, SAND80-0984 (Albuquerque, NM: Sandia National Laboratories, 1980).
- <sup>5</sup>R. E. Akins, *Wind Characteristics for Field Testing of Wind Energy Conversion Systems*, SAND78-1563 (Albuquerque, NM: Sandia National Laboratories, 1978).
- <sup>6</sup>R. E. Akins, *Wind Characteristics at the VAWT Test Facility*, SAND78-0760 (Albuquerque, NM: Sandia National Laboratories, 1978).
- <sup>7</sup>R. E. Akins, *Performance Evaluation of Wind Energy Conversion Systems Using the Method of Bins—Current Status*, SAND77-1375 (Albuquerque, NM: Sandia National Laboratories, 1978).
- <sup>8</sup>R. E. Akins, "Method-of-Bins Update," *Proceedings of Wind Energy Expo '82* (Amarillo, TX: American Wind Energy Association, October 1982).
- <sup>9</sup>T. E. Hausfeld and C. A. Hansen, "A Systematic Approach to Using the Method of Bins," *Proceedings of the Sixth Biennial Wind Energy Conference* (Minneapolis, MN: American Solar Energy Society, June 1983).
- <sup>10</sup>J. H. Strickland, B. T. Webster, and T. Nguyen, *A Vortex Model of the Darrieus Turbine: An Analytical and Experimental Study*, SAND79-7058 (Albuquerque, NM: Sandia National Laboratories, 1980).
- <sup>11</sup>D. E. Berg, "Recent Improvements to the VDART3 VAWT Code," *1983 Wind/Solar Energy Conference* (Kansas City, MO: University of Missouri-Columbia, April 1983).
- <sup>12</sup>R. E. Gormont, *A Mathematical Model of Unsteady Aerodynamics and Radial Flow for Application to Helicopter Rotors*, USAAMRDL Technical Report 72-67 (Philadelphia, PA: Boeing Company, 1973).
- <sup>13</sup>B. Massé, *Description de deux programmes d'ordinateur pour le calcul des performances et des charges aérodynamiques pour les éoliennes à axe vertical*, IREQ-2379 (Varenes, Canada: Institut de Recherche d'Hydro-Québec, 1981).

DISTRIBUTION:

ALCOA Technical Center (5)  
Aluminum Company of America  
Attn: D. K. Ai  
J. T. Huang  
J. R. Jombock  
M. Klingensmith  
J. L. Prohaska  
Alcoa Center, PA 15069

Alternative Sources of Energy  
Attn: L. Stoiaken  
Milaca, MN 56353

Amarillo College  
Attn: E. Gilmore  
Amarillo, TX 79100

American Wind Energy Association  
1017 King Street  
Alexandria, VA 22314

Arizona State University  
Attn: M. E. Beecher  
University Library  
Tempe, AZ 85281

Trinity Western  
Attn: Dr. A. S. Barker  
7600 Glover Road  
Langley, BC  
CANADA V3A 4R9

Battelle-Pacific Northwest Laboratory  
Attn: L. Wendell  
PO Box 999  
Richland, WA 99352

Bechtel Group, Inc.  
Attn: B. Lessley  
PO Box 3965  
San Francisco, CA 94119

National Technical University  
Attn: Dr. George Bergeles  
Dept. of Mechanical Engineering  
42, Patission Street  
Athens, GREECE

Bonneville Power Administration  
Attn: N. Butler  
PO Box 3621  
Portland, OR 97208

Burns & Roe, Inc.  
Attn: G. A. Fontana  
800 Kinderkamack Road  
Oradell, NJ 07649

Canadian Standards Association  
Attn: T. Watson  
178 Rexdale Blvd.  
Rexdale, Ontario, M9W 1R3  
CANADA

National Research Council of Canada  
Attn: Mark Chappel  
Division of Energy  
Montreal Road  
Ottawa, Ontario  
CANADA K1A 0R6

University of Auckland  
Attn: Prof. V. A. L. Chasteau  
School of Engineering  
Private Bag  
Auckland, NEW ZEALAND

Colorado State University  
Attn: R. N. Meroney  
Dept. of Civil Engineering  
Fort Collins, CO 80521

Commonwealth Electric Co.  
Attn: D. W. Dunham  
Box 368  
Vineyard Haven, MA 02568

Curtis Associates  
Attn: Gale B. Curtis  
3089 Oro Blanco Drive  
Colorado Springs, CO 80917

M. M. Curvin  
11169 Loop Road  
Soddy Daisy, TN 37379

Dept. of Economic Planning and Development  
Attn: G. N. Monsson  
Barrett Building  
Cheyenne, WY 82002

National Aerospace Laboratory  
Attn: Otto deVries  
Anthony Fokkerweg 2  
Amsterdam 1017  
THE NETHERLANDS

DISTRIBUTION (Continued):

DOE/ALO

Attn: G. P. Tennyson  
Albuquerque, NM 87115

DOE/ALO

Attn: Capt. J. L. Hanson, USAF  
Energy Technology Liaison Office  
NGD  
Albuquerque, NM 87115

DOE Headquarters (20)

Wind/Oceans Technologies Div.  
Attn: P. R. Goldman  
L. J. Rogers  
1000 Independence Ave.  
Washington, DC 20585

Nederlands Energy Research Foundation  
(E.C.N.)

Attn: J. B. Dragt  
Physics Department  
Westerduinweg 3 Petten (nh)  
THE NETHERLANDS

Dynergy Systems Corporation

Attn: C. Fagundes  
821 West L Street  
Los Banos, CA 93635

Electric Power Research Institute (2)

Attn: E. Demeo  
F. Goodman  
3412 Hillview Avenue  
Palo Alto, CA 94304

Dr. Norman E. Farb

10705 Providence Drive  
Villa Park, CA 92667

Pontificia Universidade Catolica-PUC/Rj

Attn: Alcir de Faro Orlando  
Mechanical Engineering Department  
R. Marques de S. Vicente 225  
Rio de Janeiro, BRAZIL

FloWind Corporation (2)

Attn: B. Im  
L. Schienbein  
1183 Quarry Lane  
Pleasanton, CA 94566

Garrad Hasson

Attn: A. D. Garrad  
10 Northampton Square  
London EC1M 5PA  
UNITED KINGDOM

Gates Learjet

Mid-Continent Airport  
Attn: G. D. Park  
PO Box 7707  
Wichita, KS 67277

H. Gerardin

Mechanical Engineering Department  
Faculty of Sciences and Engineering  
Université Laval-Québec, G1K 7P4  
CANADA

University College of Swansea

Attn: R. T. Griffiths  
Dept. of Mechanical Engineering  
Singleton Park  
Swansea, SA2 8PP  
UNITED KINGDOM

Helion, Inc.

Attn: J. Park, President  
Box 445  
Brownsville, CA 95919

Indal Technologies, Inc. (2)

Attn: D. Malcolm  
C. Wood  
3570 Hawkestone Road  
Mississauga, Ontario  
CANADA L5C 2V8

Institut de Recherche d'Hydro-Québec (2)

Attn: Gaston Beaulieu  
Bernard Massé  
1800, Montee Ste-Julie  
Varenes, Québec, JOL 2P.O.  
CANADA

Iowa State University

Attn: L. H. Soderholm  
Agricultural Engineering, Room 213  
Ames, IA 50010

West Wind Industries

Attn: K. Jackson  
PO Box 1705  
Davis, CA 95617

DISTRIBUTION (Continued):

McAllester Financial  
Attn: M. Jackson  
1816 Summit  
W. Lafayette, IN 47906

Kaiser Aluminum & Chemical Sales, Inc.  
Attn: A. A. Hagman  
14200 Cottage Grove Avenue  
Dolton, IL 60419

Kaiser Aluminum & Chemical Sales, Inc.  
Attn: D. D. Doerr  
6177 Sunol Blvd.  
PO Box 877  
Pleasanton, CA 94566

Kansas State University  
Attn: Dr. G. L. Johnson  
Electrical Engineering Dept.  
Manhattan, KS 66506

The College of Trades and Technology  
Attn: R. E. Kelland  
PO Box 1693  
Prince Philip Drive  
St. John's, Newfoundland, A1C 5P7  
CANADA

KW Control Systems, Inc.  
Attn: R. H. Klein  
RD#4, Box 914C  
South Plank Road  
Middletown, NY 10940

Kalman Nagy Lehoczky  
Cort Adellers GT. 30  
Oslo 2, NORWAY

L. K. Liljergren  
1260 S.E. Walnut #5  
Tustin, CA 92680

L. Liljidahl  
Building 005, Room 304  
Barc-West  
Beltsville, MD 20705

Olle Ljungstrom  
FFA, The Aeronautical Research Institute  
Box 11021  
S-16111 Bromma, SWEDEN

R. Lynette & Associates, Inc.  
Attn: Robert Lynette  
15042 NE 40th Street, Ste. 206  
Redmond, WA 98052

Massachusetts Institute of Technology (2)  
Attn: Prof. N. D. Ham  
W. L. Harris, Aero/Astro Dept.  
77 Massachusetts Avenue  
Cambridge, MA 02139

H. S. Matsuda  
Composite Materials Laboratory  
Pioneering R&D Laboratories  
Toray Industries, Inc.  
Sonoyama, Otsu, Shiga, JAPAN 520

US Wind Power  
Attn: G. M. McNerney  
160 Wheeler Road  
Burlington, MA 01803

Michigan State University  
Attn: O. Krauss  
Div. of Engineering Research  
East Lansing, MI 48825

Napier College of Commerce and Technology  
Tutor Librarian, Technology Faculty  
Colinton Road  
Edinburgh, EH10 5DT  
ENGLAND

National Rural Electric Cooperative Assn.  
Attn: Wilson Prichett, III  
1800 Massachusetts Avenue, NW  
Washington, DC 20036

Natural Power, Inc.  
Attn: Leander Nichols  
New Boston, NH 03070

Northwestern University  
Attn: R. A. Parmalee  
Dept. of Civil Engineering  
Evanston, IL 60201

Ohio State University  
Attn: Prof. G. Gregorek  
Aeronautical and Astronautical Dept.  
2070 Neil Avenue  
Columbus, OH 43210

DISTRIBUTION (Continued):

Oklahoma State University  
Attn: D. K. McLaughlin  
Mechanical Engineering Dept.  
Stillwater, OK 76074

Oregon State University  
Attn: R. E. Wilson  
Mechanical Engineering Dept.  
Corvallis, OR 97331

Pacific Gas & Electric Co.  
Attn: T. Hillesland  
3400 Crow Canyon Road  
San Ramon, CA 94583

Ion Paraschivoiu  
Dept. of Mechanical Engineering  
École Polytechnique  
CP 6079  
Succursale A  
Montreal H3C 3A7  
CANADA

Jacques Plante  
Hydro-Québec  
Place Dupuis II<sup>e</sup> étage  
855 est rue Ste-Catherine  
Montreal, Québec  
CANADA H2L 4P5

The Power Company, Inc.  
Attn: A. A. Nedd  
PO Box 221  
Genesee Depot, WI 53217

Power Technologies, Inc.  
Attn: Eric N. Hinrichsen  
PO Box 1058  
Schenectady, NY 12301-1058

Public Service Co. of New Hampshire  
Attn: D. L. C. Frederick  
1000 Elm Street  
Manchester, NH 03105

Public Service Co. of New Mexico  
Attn: M. Lechner  
PO Box 2267  
Albuquerque, NM 87103

RANN, Inc.  
Attn: A. J. Eggers, Jr.  
260 Sheridan Ave., Suite 414  
Palo Alto, CA 94306

Iowa State University  
Attn: Dr. R. Ganesh Rajagopalan  
Aerospace Engineering Dept.  
404 Town Engineering Bldg.  
Ames, IA 50011

The Resources Agency  
Dept. of Water Resources Energy Div.  
Attn: R. G. Ferreira  
PO Box 388  
Sacramento, CA 95802

Reynolds Metals Company  
Mill Products Division  
Attn: G. E. Lennox  
6601 West Broad Street  
Richmond, VA 23261

R. G. Richards  
Atlantic Wind Test Site  
PO Box 189  
Tignish P.E.I., COB 2B0  
CANADA

Riso National Laboratory (2)  
Attn: Troels Friis Pedersen  
Helge Petersen  
Postbox 49  
DK-4000 Roskilde  
DENMARK

Memorial University of Newfoundland  
Attn: A. Robb  
Faculty of Eng. and Applied Sciences  
St. John's Newfoundland, A1C 5S7  
CANADA

Dr. Ing. Hans Ruscheweyh  
Institut für Leichbau  
Technische Hochschule Aachen  
Wullnerstrasse 7  
FEDERAL REPUBLIC OF GERMANY

Beatrice de Saint Louvent  
Etablissement d'Etudes et de Recherches  
Météorologiques  
77 rue de Serves  
92106 Boulogne-Billancourt Cédex  
FRANCE

DISTRIBUTION (Continued):

National Atomic Museum  
Attn: Gwen Schreiner, Librarian  
Albuquerque, NM 87115

Arnan Seginer, Professor of Aerodynamics  
Technion-Israel Institute of Technology  
Dept. of Aeronautical Engineering  
Haifa  
ISRAEL

Wind Energy Abstracts  
Attn: Farrell Smith Seiler, Editor  
PO Box 3870  
Bozeman, MT 59772-3870

David Sharpe  
Dept. of Aeronautical Engineering  
Queen Mary College  
Mile End Road  
London, E1 4NS  
UNITED KINGDOM

Kent Smith  
Instituto Tecnológico Costa Rico  
Apartado 159 Cartago  
COSTA RICA

Solar Energy Research Institute  
Attn: R. W. Thresher  
1617 Cole Boulevard  
Golden, CO 80401

Bent Sorenson  
Roskilde University Center  
Energy Group, Bldg. 17.2  
IMFUFA  
PO Box 260  
DK-400 Roskilde  
DENMARK

Peter South  
ADECON  
32 Rivalda Road  
Weston, Ontario, M9M 2M3  
CANADA

Southern California Edison  
Research & Development Dept., Room 497  
Attn: R. L. Scheffler  
PO Box 800  
Rosemead, CA 91770

G. Stacey  
The University of Reading  
Department of Engineering  
Whiteknights, Reading, RG6 2AY  
ENGLAND

Stanford University  
Attn: Holt Ashley  
Dept. of Aeronautics and  
Astronautics Mechanical Engineering  
Stanford, CA 94305

Dr. Derek Taylor  
Alternative Energy Group  
Walton Hall  
Open University  
Milton Keynes, MK7 6AA  
UNITED KINGDOM

R. J. Templin (3)  
Low-Speed Aerodynamics Laboratory  
NRC-National Aeronautical Establishment  
Montreal Road  
Ottawa, Ontario, K1A 0R6  
CANADA

Texas Tech University (2)  
Attn: J. W. Oler  
Mechanical Engineering Dept.  
PO Box 4289  
Lubbock, TX 79409

Moriah Research  
Attn: K. J. Touryan  
6200 Plateau Dr.  
Englewood, CO 80111

Tulane University  
Attn: R. G. Watts  
Dept. of Mechanical Engineering  
New Orleans, LA 70018

Tumac Industries, Inc.  
Attn: J. R. McConnell  
650 Ford Street  
Colorado Springs, CO 80915

J. M. Turner  
Terrestrial Energy Technology Program  
Energy Conversion Branch  
Aerospace Power Div./Aero Propulsion Lab  
Air Force Systems Command (AFSC)  
Wright-Patterson AFB, OH 45433

DISTRIBUTION (Continued):

United Engineers and Constructors, Inc.  
Attn: A. J. Karalis  
PO Box 8223  
Philadelphia, PA 19101

Universal Data Systems  
Attn: C. W. Dodd  
5000 Bradford Drive  
Huntsville, AL 35805

University of California  
Institute of Geophysics and  
Planetary Physics  
Attn: Dr. P. J. Baum  
Riverside, CA 92521

University of Colorado  
Attn: J. D. Fock, Jr.  
Dept. of Aerospace Engineering Sciences  
Boulder, CO 80309

University of Massachusetts  
Attn: Dr. D. E. Cromack  
Mechanical & Aerospace Eng. Dept.  
Amherst, MA 01003

Bureau of Engineering Research (2)  
University of New Mexico  
Attn: W. T. Cyrus  
G. G. Leigh  
Campus PO Box 25  
Albuquerque, NM 87131

University of Oklahoma  
Attn: K. Bergey  
Aero Engineering Department  
Norman, OK 73069

University of Sherbrooke (2)  
Attn: A. Laneville  
P. Vittecoq  
Faculty of Applied Science  
Sherbrooke, Québec, J1K 2R1  
CANADA

The University of Tennessee  
Attn: T. W. Reddoch  
Dept. of Electrical Engineering  
Knoxville, TN 37916

USDA, Agricultural Research Service  
Southwest Great Plains Research Center  
Attn: Dr. R. N. Clark  
Bushland, TX 79012

Utah Power and Light Co.  
Attn: K. R. Rasmussen  
51 East Main Street  
PO Box 277  
American Fork, UT 84003

W. A. Vachon  
W. A. Vachon & Associates  
PO Box 149  
Manchester, MA 01944

Dirk Vandenberghe  
State University of Ghent  
St. Pietersnieuwstraat 41  
9000 Ghent  
BELGIUM

Washington and Lee University  
Attn: Dr. R. E. Akins  
PO Box 735  
Lexington, VA 24450

Washington State University  
Attn: F. K. Bechtel  
Dept. of Electrical Engineering  
Pullman, WA 99163

West Texas State University  
Government Depository Library  
Number 613  
Canyon, TX 79015

West Texas State University  
Attn: V. Nelson  
Department of Physics  
PO Box 248  
Canyon, TX 79016

West Virginia University  
Attn: R. Walters  
Dept. of Aero Engineering  
1062 Kountz Avenue  
Morgantown, WV 26505

Central Lincoln People's Utility District  
Attn: D. Westlind  
2129 North Coast Highway  
Newport, OR 97365-1795

DISTRIBUTION (Concluded):

Wichita State University (2)  
Attn: M. Snyder  
W. Wentz  
Aero Engineering Department  
Wichita, KS 67208

Wind Power Digest  
Attn: Michael Evans  
PO Box 700  
Bascom, OH 44809

Wisconsin Division of State Energy  
Attn: Wind Program Manager  
101 South Webster St., 8th Floor  
Madison, WI 53702

1520 C. W. Peterson  
1522 R. C. Reuter, Jr.  
1523 J. H. Biffle  
1524 A. K. Miller  
1524 D. W. Lobitz  
1550 R. C. Maydew  
1556 G. F. Homicz  
2525 R. P. Clark  
3160 J. E. Mitchell (15)  
3162 P. S. Wilson  
6000 D. L. Hartley

6200 V. L. Dugan  
6220 D. G. Schueler  
6225 T. D. Ashwill  
6225 D. E. Berg  
6225 T. C. Bryant  
6225 H. M. Dodd (50)  
6225 L. R. Gallo  
6225 P. C. Klimas  
6225 S. D. Nicolaysen  
6225 D. S. Oscar  
6225 M. E. Ralph  
6225 D. C. Reda  
6225 M. A. Rumsey  
6225 L. L. Schluter  
6225 W. A. Stephenson  
6225 H. J. Sutherland  
7111 J. W. Reed  
7544 T. G. Carne  
7544 J. P. Lauffer  
9100 R. G. Clem  
9122 T. M. Leonard  
8024 P. W. Dean  
3141 S. A. Landenberger (5)  
3151 W. L. Garner (3)  
3154-1 C. H. Dalin (28)  
For DOE/OSTI (Unlimited Release)